

Chemical Evolution of Metal in Refractory Inclusions in CV3 Chondrites

ANDREW J. CAMPBELL^{*1}, STEVEN B. SIMON¹, MUNIR HUMAYUN¹, AND

LAWRENCE GROSSMAN^{1,2}

¹Department of the Geophysical Sciences,

²and Enrico Fermi Institute,

The University of Chicago, Chicago, Illinois 60637 USA

*email: acampbel@midway.uchicago.edu

ph: (773) 834-1523, fax: (773) 702-9505

Submitted to *Geochim. Cosmochim. Acta*: July 16, 2001

Revised: November 5, 2001

Accepted: December 1, 2001 for Special Issue in Honor of R. N. Clayton

Abstract—Laser ablation inductively coupled plasma mass spectrometry (LA-ICP-MS) was used to measure distributions of the siderophile elements V, Fe, Co, Ni, Mo, Ru, Rh, Pd, W, Re, Os, Ir, Pt, and Au in Fremdlinge with a spatial resolution of 15-25 μm . A sulfide vein in a refractory inclusion in Allende (CV3-oxidized) is enriched in Rh, Ru, and Os with no detectable Pd, Re, Ir, or Pt, indicating that Rh, Ru, and Os were redistributed by sulfidation of the inclusion, causing fractionation of Re/Os and other siderophile element ratios in Allende CAIs. Fremdlinge in compact type A inclusions from Efremovka (CV3-reduced) exhibit subsolidus exsolution into kamacite and taenite, and minimal secondary formation of V-magnetite and schreibersite. Siderophile element partitioning between taenite and kamacite is similar to that observed previously in iron meteorites, while preferential incorporation of the light PGEs (Ru, Rh, Pd) relative to Re, Os, Ir and Pt by schreibersite was observed. Fremdling EM2 (CAI Ef2) has an outer rim of P-free metal that preserves the PGE signature of schreibersite, indicating that EM2 originally had a phosphide rim, and lost P to the surrounding inclusion during secondary processing. Most Fremdlinge have chondrite-normalized refractory PGE patterns that are unfractionated, with PGE abundances derived from a small range of condensation temperatures, approximately 1480-1468 K at $P_{\text{tot}} = 10^{-3}$ bar. Some Fremdlinge from the same CAI exhibit sloping PGE abundance patterns, and Re/Os ratios up to $2x_{\text{CI}}$, that likely represent mixing of grains that condensed at various temperatures.

1. INTRODUCTION

Calcium, aluminum-rich inclusions (CAIs) are refractory solids that condensed early in the solar nebula (Grossman, 1972; 1980). The presence of oxygen isotopic anomalies in Allende CAIs (Clayton et al., 1973) stimulated many further investigations of isotopic compositions of O, Mg, Si, Ca, Ti, and refractory siderophiles (e.g., Clayton et al., 1977; 1988; Hutcheon et al. 1987) in search of nuclear anomalies and extinct radioactivities. Isotopic studies of Mg (Wasserburg et al., 1977) and Si (Clayton et al., 1978) revealed the presence of mass dependent fractionations indicating that Compact Type A (CTA) and Type B CAIs had experienced evaporative losses of their major constituents (Clayton et al., 1985; 1988). Chronological studies of processes in the early solar nebula have also focussed on CAIs (e.g., Podosek et al., 1991), including a recent effort using the siderophile Re-Os system (Becker et al., 2001).

Elemental distributions have been extensively studied to determine the processes of formation of CAIs, including both condensation from a gas of solar composition (Grossman, 1972; Davis and Grossman, 1979), and subsequent evaporation during melting to form CTA and Type B CAIs (Grossman et al., 2000; 2001). In Allende CAIs, refractory lithophiles are concentrated in the silicate and oxide phases that make up the bulk of the inclusions, whereas refractory siderophiles such as the platinum group elements (PGEs: Ru, Rh, Pd, Os, Ir, Pt), Re, W, and Mo are found in very high concentrations in isolated refractory metal nuggets (Wark, 1986) and in metal-rich, opaque assemblages known as Fremdlinge (El Goresy et al., 1978; Grossman, 1980). Grossman et al. (2000; 2001) described the control of major element and isotopic compositions of CAIs by high-temperature condensation of silicates, followed by loss of Mg and Si by evaporation of the molten droplets into the surrounding H₂ gas.

Fremdlinge were originally interpreted as high-temperature condensates that were later incorporated into their host inclusions (El Goresy et al., 1978). Subsequent

investigators, calling the metal-rich nodules “opaque assemblages,” expanded that view based on phase equilibrium studies in the Ni-Fe-Ru, Ni-Fe-S, and Ni-Fe-O systems (Blum et al., 1988; 1989a,b). They argued that homogeneous metallic grains formed during melting of CAIs, and that these alloys were later subject to exsolution, sulfidation, and oxidation at lower temperatures, forming the assemblages now observed (Blum et al., 1989b). Sylvester et al. (1990) used instrumental neutron activation analysis (INAA) to determine the siderophile element abundances of Fremdlinge in a Type B CAI from Allende. They interpreted their results in the framework of multiple alloy condensation; varying siderophile element concentrations were attributed to varying condensation temperatures and modal proportions of the constituent alloys. Palme et al. (1994) emphasized the difference in PGE abundance patterns of bulk Fremdlinge from a single inclusion. They observed that different Fremdlinge from the same inclusion displayed PGE patterns that were different from one another, and that these patterns were volatility-related. They concluded that the Fremdlinge must have formed prior to incorporation into CAIs, as opposed to the aggregation of homogeneous alloys pictured by Blum et al. (1989b).

Some of the difficulty in interpretation of Fremdling compositions is related to the late-stage sulfidation and oxidation that was examined by Blum et al. (1989b). Most of the work on the subject of Fremdling formation has been done on CAIs from Allende, a member of the oxidized subgroup of CV3 chondrites. It is widely recognized, however, that CAIs from the reduced subgroup of CV3 chondrites were subjected to much less of the late-stage processing that complicates Fremdling studies (MacPherson et al., 1988). In this work, we have examined a sulfide vein in an Allende CAI to investigate the mobility of siderophile elements during secondary sulfidation. Further, we have focussed on Fremdlinge from Efremovka (CV3-reduced), to avoid these difficulties as much as possible and to better interpret the nebular aspects of Fremdling origins.

Previous measurements of PGE abundances in Fremdlinge used neutron activation analysis on bulk Fremdlinge, or electron microprobe analysis of individual minerals within

Fremdlinge; the latter studies were limited by the sensitivity of the microprobe to platinum group elements, with detection limits of ~1000 ppm. Laser ablation ICP-MS was used in this study to measure siderophile element concentrations in Fremdlinge with a spatial resolution as low as ~15 μm and detection limits <1 ppm in most cases. These experiments allow comparisons of siderophile concentrations to be made not only between Fremdlinge but also between individual phases or locations within a Fremdling, and with sufficient sensitivity to determine trace element concentrations in nearly all Fremdlinge, not only those with the most elevated abundances. Data are presented for a sulfide-rich vein in an Allende CAI, and for 26 Fremdlinge from three compact type A (melilite-rich) CAIs in Efremovka (CV3-reduced). Preliminary results of this study were presented in Campbell et al. (1999).

2. EXPERIMENTAL

Four compact type A inclusions were studied: TS68 from Allende, and Ef1, Ef2, and Ef3 from Efremovka. Sections of each CAI were carbon coated and examined using a JEOL 5800LV SEM and a Cameca SX-50 electron microprobe prior to LA-ICP-MS analysis. Metal grains were selected for further examination based on their size and mineralogy.

The laser ablation system utilized a CETAC LSX-200 laser ablation peripheral with a Finnigan MAT Element ICP mass spectrometer (Campbell and Humayun, 1999a,b). The LSX-200 has been upgraded since the work of Campbell and Humayun (1999a). The microscope objective lens was increased in magnification from 5X to 10X; this allowed higher power densities of laser light to be focussed onto the sample, improving ablation efficiency and increasing sensitivity. Also, the method of adjusting the beam diameter has been changed from a beam expander to a variable aperture system. This change has

produced better ablation pit morphologies, improving spatial resolution without sacrificing signal intensity.

The isotopes measured were ^{31}P , ^{34}S , ^{51}V , ^{57}Fe , ^{59}Co , ^{60}Ni , ^{95}Mo , ^{101}Ru , ^{103}Rh , ^{105}Pd , ^{182}W , ^{187}Re , ^{192}Os , ^{193}Ir , ^{195}Pt , and ^{197}Au . Instrumental sensitivity factors for each isotope were determined by measuring signal intensity from the group IVB iron meteorite Hoba, a synthetic pyrrhotite standard, and the NIST reference material SRM 612, which have known concentrations of the elements of interest (Campbell and Humayun, 1999b; Campbell et al., 2001a). Each point on the sample was ablated by 15 laser pulses at 10 Hz; most laser-ablated pits produced were 15 μm in diameter and approximately 8 μm deep; a few points were analyzed with a 25 μm diameter spot instead. The mass spectrometer was swept over the entire mass range every 0.664 s, while the ablated material was carried by Ar gas from the sample chamber to the mass spectrometer. The signal from the transient laser ablation pulse was integrated over a period of 26.6 s (40 mass cycles); this was sufficient time for the pulse to reach a peak intensity and then decay almost to background levels. Typical time-averaged signal intensities for 500 ppm $^{193}\text{Ir}^+$ were $\sim 10,000$ cps, with a background of ~ 1 cps.

Uncertainties reflect contributions from counting statistics as well as an instrumental error, that is largely due to the transience of the signal. The counting errors incorporate both the measured counts and the counts in the blank measurement. The instrumental error was calculated from repeat measurements of the Hoba standard, by stripping away the counting errors from the standard deviations. This is a conservative estimate of the instrumental error because it includes the effects of heterogeneity in Hoba, which is an ataxite consisting primarily of a fine plessitic intergrowth with a few ~ 20 μm wide kamacite spindles. Instrumental errors (2σ) were assigned as 11% for PGEs and 5% for major and minor elements; these are average values from seven different calibrations.

3. RESULTS

3.1. Sulfide Vein in Refractory Inclusion TS68 of Allende

In Allende CAIs metal- and sulfide-rich veins are commonly associated with Fremdlinge; in polished sections they are often observed in cracks that cross-cut Fremdlinge. Campbell et al. (1999) showed a LA-ICP-MS scan across a sulfide vein in an Allende CAI, TS68, that was studied earlier by Sylvester et al. (1992) and Simon et al. (1999). The mean composition of this vein is given in Table 1. Several elements, including V, Mo, Ru, Rh, W and Os, show enrichment in this vein. The enrichment of Ru is greater than that of Rh and Os; other PGEs were not detected in the vein.

3.2 Microdistribution of Siderophile Elements in Efremovka Fremdlinge

Three sections of Efremovka CAIs were examined. The first consists of a single large Fremdling, EM1, that had been separated from inclusion Ef1. The second, Ef2, was described earlier by Fisenko et al. (1992); it contains one large Fremdling (EM2) and numerous Fremdlinge that all measure <50 μm in size (Figure 1). The small Fremdlinge in this section are typically rounded, sometimes irregular, and commonly associated with spinel grains. A few small metal veinlets were also observed. Section Ef3 was described previously by Sylvester et al. (1993) and by Simon et al. (1999). It also contains one large Fremdling and numerous smaller Fremdlinge. The distribution of these Fremdlinge is similar to that in Ef2, with the small Fremdlinge often associated with spinel. Micron-sized refractory metal nuggets, such as those in Allende reported by El Goresy et al. (1978) and by Wark (1986), were not observed in any of the Efremovka sections studied.

A backscattered electron image of a large Fremdling in the Efremovka CAI Ef3 is shown in Figure 2. This Fremdling, previously described and named "The Heart" by

Casanova and Grossman (1993), consists of a fine intergrowth of kamacite and taenite, with accessory vanadian magnetite present as 0.5-5 μm grains. A large phosphate vein is present on the right hand side of the Fremdling in Figure 2. Five points in The Heart were analyzed by LA-ICP-MS with a spatial resolution of 25 μm , and their locations are indicated in Figure 2. The results are presented in Table 2, and siderophile element abundance patterns, normalized to Ni and CI chondrites, are shown in Figure 3. Due to the fine intergrowth of kamacite, taenite, and vanadian magnetite, each LA-ICP-MS measurement sampled an unknown mixture of the three components. As shown in Figure 2, however, it is expected that point #3 included a higher fraction of oxide than the other points. The relative abundances of Re, Os, Ir, Ru, Pt, and Rh are nearly chondritic in this Fremdling, and the Ni-normalized abundances of these highly siderophile elements (HSEs) are enriched by 20X - 200X chondritic (Figure 3). Variations in the normalized refractory PGE abundances (Figure 3) primarily reflect variations in the Ni content (Table 2), which result from differences in the kamacite/taenite proportions sampled at each point (Figure 2). The relatively volatile element Pd, however, is strongly depleted relative to other PGEs; W and Mo are also depleted.

EM1, pictured in Figure 4, is a Fremdling in Efremovka CAI Ef1 measuring ~ 600 μm across. It consists principally of taenite (49 vol%), with numerous exsolved kamacite grains with widths of 1-50 μm and lengths of approximately 5-150 μm . EM1 has 42 vol% kamacite, 7 vol% schreibersite (8-40 μm equant grains), and 1 vol% of vanadium-rich oxide and sulfides (5-15 μm). LA-ICP-MS analyses of individual phases in EM1, with a spatial resolution of 15 μm , are presented in Table 3 and the CI-normalized HSE patterns are shown in Figure 5. The sulfide grains are small relative to the laser spot size, and the “V-sulfide” analyses in Table 3 and Figure 5 represent an uncertain mixture of V-rich sulfides, oxide and metal; therefore it is unsurprising that most siderophile element concentrations are similar to those in taenite. However, Mo and V show large enrichments in these analyses. Microprobe analyses of the sulfides (Table 4) revealed two different

stoichiometries: approximately $(\text{Fe},\text{Mo})\text{V}_2\text{S}_4$ and $(\text{Fe},\text{Mo},\text{V})_{11}\text{S}_{12}$. These two phases, and the less abundant V-rich oxide, frequently occur in contact with one another.

Kamacite and taenite exhibit approximately flat patterns for the refractory PGEs in EM1 (Figure 5). Molybdenum is less strongly enriched than the refractory PGEs in the kamacite; minor sulfide inclusions may have contributed to the Mo and V abundances observed in taenite (Table 4). The abundances of the remaining siderophiles (Ni, Co, Fe, Pd, Au) in the metal phases are lower than those of the refractory elements, indicating a trend of decreasing concentration with volatility. Strong Co/Ni fractionation is evident between taenite and kamacite; this is consistent with expectations based on taenite/kamacite partitioning observed in iron meteorites (Buchwald, 1975). The refractory PGEs do not partition strongly between taenite and kamacite (Campbell and Humayun, 1999b); the difference in Ni-normalized abundances seen in Figure 5 is an artifact of the Ni partitioning between the two phases. The schreibersite data in Figure 5 show strong enrichment in the light PGEs (Ru, Rh) relative to the heavy PGEs (Os, Ir, Pt) and Re, compared to the associated metal phases. $K^{\text{tae/sch}}$ values for heavy PGEs are 300-600 and only 0.9-5 for light PGEs (Table 3). Schreibersite is also notably depleted in V ($K^{\text{tae/sch}} = 14$).

A detailed study of Fremdling EM2, in Efremovka CAI Ef2, was also carried out. This specimen consists principally of Ni-rich (~55 wt%) metal, presumably tetrataenite, with accessory phases zoned concentrically within the ~350 μm diameter Fremdling (Figures 6 and 7). In the interior of the Fremdling, schreibersite grains (2-10 μm), smaller ($\leq 1 \mu\text{m}$) V-rich magnetites, and Fe,Mo,W-bearing alloy grains ($< 2 \mu\text{m}$) are enclosed in taenite, while the outermost rim, $\leq 30 \mu\text{m}$ wide, is composed strictly of taenite. In some places outside the rim there also exists an irregular shell of phosphate between the Fremdling and the surrounding silicate (Figure 7). LA-ICP-MS measurements of each region were made using a spatial resolution of 15 μm (Table 5). The siderophile element abundance patterns in the interior of the Fremdling are shown in Figure 8 to have a systematic enrichment anticorrelated with the volatility of the elements. The rim shows a

more complicated pattern; the heavy PGEs (Re, Os, Ir, Pt) are all depleted relative to the interior, while the light PGEs (Ru, Rh, Pd) have concentrations similar to those in the interior. The elements W, Mo, and V are also depleted in the rim (Figure 8).

3.3. Bulk Compositions of Fremdlinge in Efremovka

Siderophile element abundances of Fremdlinge in inclusions Ef2 and Ef3 are listed in Table 6, and their Ni, CI-normalized abundance patterns are shown in Figure 9. Most of the entries in this table consist of measurements made on Fremdlinge that were too small for analyses to be carried out on individual phases; it is assumed that these analyses are representative of the bulk compositions of the Fremdlinge. Calculated bulk abundances for each of the large Fremdlinge discussed above (The Heart in Ef3, EM1 in Ef1, and EM2 in Ef2) are also illustrated (Figure 9C). Most Fremdlinge in these three CAIs have approximately flat refractory PGE patterns, although EM13 (Ef2), like EM2 (Ef2), has a sloping pattern of volatile depletion. Depletions in Mo and W, relative to the refractory PGEs, are often present; these are more common and of greater magnitude for Mo than for W. EM18 (Ef2) is depleted in the heavy PGEs relative to the light PGEs, similarly to the schreibersite of EM1 in Ef1 (Figure 5) and the rim of EM2 in Ef2 (Figure 8).

4. DISCUSSION

4.1. Secondary Sulfidation and Siderophile Element Redistribution in Allende

Blum et al. (1988, 1989a) proposed a model for Fremdling formation that begins with accumulation of numerous fine metal particles in an aggregating CAI. Upon melting of the CAI, metal droplets coalesce to form proto-Fremdlings. Later subsolidus exsolution, oxidation and sulfidation in higher than solar $f(\text{O}_2)$, $f(\text{S}_2)$ conditions, either in the nebula or on a parent body, then produce the textures observed in CAI metal. This interpretation was supported in part by diffusion and phase equilibrium experiments in the Ni-Fe-Ru system (Blum et al., 1989b). The framework of Blum et al. (1988, 1989a) can explain the observed mineralogy of individual Fremdlings, but it does not explicitly account for the wide variation of PGE contents observed among Fremdlings within a single CAI; specifically, it does not explain how Fremdlings that coalesced from the same population of many fine metal particles did not converge to the same PGE abundances or patterns (Bischoff and Palme, 1987; Sylvester et al., 1990; Palme et al., 1994).

Most Fremdlings that have been studied are from CAIs in the CV3 meteorite Allende. Allende is a member of the “oxidized” subgroup of CV3 meteorites (McSween, 1977; Weisberg et al., 1997), and Allende CAIs generally have undergone a greater degree of the late-stage oxidation and sulfidation that Blum et al. (1989a) describe than inclusions from the “reduced” CV3 subgroup. The effect of this late-stage processing on the PGE distributions is evident from the LA-ICP-MS measurements on a sulfide vein in the silicate portion of Allende CAI TS68 (Table 1). The PGEs and other siderophiles have been redistributed from the Fremdlings by the sulfide veins in this inclusion, thus obscuring the original metal compositions. These observations are consistent with those of Sylvester et al. (1992), who previously noted Ru enrichments in electron microprobe analyses of

sulfide veins in Allende CAIs. The concentration of W in the vein is also noteworthy (Table 1); W is less chalcophile than Mo, and the enrichment of W in the vein relative to Mo may indicate oxidation as well as sulfidation during vein formation. A possible additional effect of the late-stage alteration of Allende CAIs is to obscure the original rounded morphology of Fremdlinge (as predominantly seen in Efremovka) during recrystallization associated with sulfide formation.

The CAI metal in Efremovka, a member of the reduced subgroup of CV3 chondrites, was subjected to less sulfidation than the CAI metal in Allende. Most Fremdlinge in Efremovka are metal grains with (at most) minor sulfide inclusions, unlike the heavily sulfidized assemblages found in Allende (e.g., Blum et al., 1989a). For example, the sulfides in EM1 in Ef1 (Figure 4) are distributed within the interior of the Fremdling, rather than concentrated on the exterior, and must reflect exsolution rather than later sulfidation of the CAI. Furthermore, the networks of sulfide veins that commonly crosscut Fremdlinge in Allende CAIs are much less extensive in Efremovka. Therefore, redistribution of PGEs by late-stage sulfidation was minimal in Efremovka CAIs. This may explain the relative paucity in Efremovka of refractory metal nuggets in Fremdlinge, like those observed in Allende, which Blum et al. (1989b) suggested may be secondary.

Recent Re-Os and highly siderophile element studies of bulk carbonaceous chondrites have emphasized the complex evolution of the Re-Os system in these meteorites. Walker et al. (2001) showed, from ^{187}Re - ^{187}Os systematics of bulk carbonaceous chondrites, that their Re/Os ratios have been disturbed by parent-body processes relatively recently, indicating mobility of one or both of the elements long after condensation from the nebula. Horan et al. (2001) showed elemental abundance patterns for the same chondrites that exhibit distinct differences from CI abundances (Anders and Grevesse, 1989) relative to Ir by 20-50% in the other HSEs, particularly Pt and Pd. The observed variations are not simple functions of condensation temperature, but reflect open-system disturbances of the HSEs by oxidation, sulfidation, etc., on parent bodies. Becker et al. (2001) determined the

Re-Os systematics of whole CAIs and powdered splits of CAIs from Allende, and found evidence for significant resetting of the Re/Os ratio, with a possible disturbance at 1.6 Ga. They concluded that the Re/Os variability resulted from late-stage, open-system behavior involving the mobilization of Re or Os in veins. In the present study we have used LA-ICP-MS to directly address the question of elemental mobility of HSEs in a veined Allende CAI. Our results (Table 1) show that the sulfide vein we analyzed exhibits HSE abundances that are highly fractionated from one another. Although Re was not detected in this vein, it is evident that Os was mobilized during sulfidation, and the strong HSE fractionations that are generally observed suggests that chondritic Re/Os ratios were not likely to be preserved during the formation of these veins. Despite the consistency between the Ru abundance in Table 1 and those reported by Sylvester et al. (1992), it should be noted that the particular HSE abundances in this vein may not be representative of all veins in the CAI. We conclude that sulfidation of Fremdling metal within a CAI mobilized the HSEs and produced veins with nonchondritic HSE ratios, including Re/Os. Subsampling of the CAI then produces fragments with variable proportions of sulfide veins and altered metal, and therefore with variable Re/Os. Such a scenario would explain the Re-Os systematics observed by Becker et al. (2001), and is consistent with their preferred interpretation, that of late-stage open-system behavior of Re and Os in an asteroidal environment.

4.2. Volatility Control of Siderophile Element Abundances in Efremovka Fremdlinge

4.2.1. Condensation Calculations

Condensate origins of Fremdlinge have been considered previously by comparing the measured abundances of the siderophile elements to those obtained through condensation calculations (Palme and Wlotzka, 1976; Blander et al., 1980; Fegley and

Palme, 1985; Sylvester et al., 1990). Palme and Wlotzka (1976) measured the bulk siderophile abundances in a single Fremdling in Allende and found that the refractory siderophiles were present at levels of $\sim 7000\times$ chondritic, whereas the less refractory siderophiles Co, Ni, and Au were not as enriched. They concluded, based on accompanying condensation calculations, that the grain had condensed from the solar nebula at a temperature between 1460 and 1500 K (assuming 10^{-3} bar total nebular pressure). Blander et al. (1980) analyzed several refractory metal nuggets having percent-level refractory siderophile contents, and only a few percent of Fe and Ni. They found that the refractory siderophile element abundances matched those of condensates from ~ 1620 K at 10^{-4} bar. The Fe and Ni contents of these grains were higher than predicted for these conditions, and it was concluded that these elements were added later to the metal grain. Fegley and Palme (1985) interpreted the depletion of Mo and W, relative to other refractory siderophiles, in CAIs and Fremdlings as being due to gaseous oxide formation in the condensing nebula. Sylvester et al. (1990) analyzed several Fremdlings from a single Allende inclusion, and found fractionations between refractory siderophiles that could not be matched with the calculated condensation path of a single alloy. Sylvester et al. (1990) invoked the condensation of multiple alloys (fcc, hcp, and bcc) to explain the observed elemental abundances. Palme et al. (1994) recognized that the high abundances of Fe, Ni, and other less refractory siderophiles in Fremdlings from an Allende inclusion implied that these elements must have condensed separately from the refractory siderophiles and were added later to the alloy.

In these previous calculations for metal condensation, as well as those below, the assumption of equilibrium is made. In this case the compositions calculated for condensation are indistinguishable from those for partial evaporation. We follow the nomenclature of earlier studies and refer to "condensation temperatures" when in fact the alloys could have formed equally well by evaporation, as long as equilibrium was reached. Possible problems associated with nucleation during condensation are also neglected in the

present calculations, because 1) the grains could have formed during evaporation, which avoids the problem entirely; 2) most of the compositions considered here are rich in Fe and Ni, and nucleation of these abundant elements is not as difficult as nucleation of PGE grains, and 3) the rate of cooling and nucleation is poorly constrained in the region of the nebula from which these alloys are envisioned to form (this contrasts with the study by Campbell et al. (2001b), in which the zoning within metal grains placed important constraints on the allowable timescales of metal condensation).

Equilibrium condensation of solid metal alloy from a solar nebula was calculated, including all of the elements that were analyzed in Fremdlinge in the present study. The calculations were carried out following previously described procedures (Grossman and Olsen, 1974; Palme and Wlotzka, 1976; Fegley and Palme, 1985; Campbell et al., 2001b). Condensation into a single alloy, with ideal solution of the HSEs, was assumed (Palme and Wlotzka, 1976; Fegley and Palme, 1985; Campbell et al., 2001b). Vapor pressure data for each element were taken from Hultgren et al. (1973) over the range 1300-2000 K. The partial pressures of oxide gases were calculated using equilibrium constants given in the JANAF tables (Chase, 1998), and the $f(\text{O}_2)$ was adapted from the work of Ebel and Grossman (2000). Except where otherwise indicated, the condensation calculations refer to a starting gas of solar composition (Anders and Grevesse, 1989), with no dust enrichment. The gaseous oxide species considered were: VO, VO₂, FeO, MoO, MoO₂, MoO₃, WO, WO₂, WO₃, W₂O₆, W₃O₈, W₃O₉, and W₄O₁₂. The equations governing equilibrium condensation were solved iteratively as described in Campbell et al. (2001b).

Results for the metallic fraction of a condensing solar nebula with $P_{\text{tot}} = 10^{-3}$ bar are presented in Figure 10, where the calculated elemental abundances in the alloy are normalized to Ni and CI chondrites to facilitate later comparison to siderophile element concentrations in Fremdlinge. As the nebular temperature drops, the CI, Ni-normalized abundances of the most refractory elements decrease in the alloy, and the abundance pattern flattens out (Figure 10A). By 1480 K the most refractory siderophile elements, Re, Os, W,

Ir, Mo, Ru, Pt, and Rh, have all completely condensed into the alloy, and no further fractionation between these elements is expected below this point in single-stage condensation (Figure 10B). Below ~1500 K the elements Fe, Ni and Co begin to condense and the normalized abundances of the refractory siderophiles quickly decrease to values near unity. At 1480 K the Fe+Ni content of the alloy is 70 wt%; by 1470 K it is >98 wt%. In Figure 10B it is shown that the normalized abundances of the refractory siderophiles drop by four orders of magnitude between 1490 K and 1460 K. In principle, the refractory siderophile element patterns of unaltered metal condensates (or evaporation residues) would provide a very sensitive thermometer of the conditions when the alloy was removed from the nebular gas (Palme and Wlotzka, 1976), if equilibrium conditions could be assumed.

The total nebular pressure, P_{tot} , was chosen in these calculations to be 10^{-3} bar, to facilitate comparison with a large body of previous work at this pressure (e.g., Grossman, 1972, 1980; Grossman and Olsen, 1974; Palme and Wlotzka, 1976; Davis and Grossman, 1979; Davis et al., 1982; Fegley and Palme, 1985; Sylvester et al., 1990; Ebel and Grossman, 2000; Grossman et al., 2000, 2001). The effect of P_{tot} is primarily to shift the temperature over which the condensation sequence occurs in the alloy. Each order of magnitude increase in P_{tot} raises the 50% condensation temperature (T_c) of each element by typically 80-100 K. The order in which the siderophiles condense into the alloy is mostly unaffected by pressure, although the maximum abundance of a given element may be sensitive to P_{tot} . The dust/gas ratio has essentially the same effect as the total pressure for those elements that do not easily form gaseous oxide species; raising the dust/gas ratio can cause a decrease in the condensed fraction of those elements (e.g., V, Mo, W) that can form stable gaseous oxides (Fegley and Palme, 1985).

4.2.2. *Condensation of Metal in CAIs*

A comparison of the refractory siderophile element patterns in Fremdlinge (Figure 9) with the calculated condensation curves (Figure 10) is instructive. With the exception of

the easily oxidizable elements W, Mo, and V, many of the refractory siderophile element patterns in the Fremdlinge studied here are approximately flat on a CI-normalized diagram, and display enrichment factors of 10-500 over chondritic abundances.

As an example, the comparison between the bulk HSE pattern of EM1 in Ef1 (Figure 9C) and the calculated abundance patterns for condensation shown in Figure 10B suggests that the metal from which EM1 formed may have last been in equilibrium with the solar nebula at a temperature of 1468 K, although the mismatch between the patterns for Pd and Co may be significant. Alternatively, the EM1 pattern may be dominated by condensates from slightly higher temperatures that mixed with (Fe,Ni)-rich metal that formed at lower temperatures. The elements Mo, V, and Fe show depletions with respect to the calculated pattern, but these elements are more easily oxidized than the others and may have been either less condensed into the alloy because of oxidizing conditions in the nebula, partitioned into co-condensing silicates and oxides, or redistributed during a later oxidation event. Alternatively, the V, Mo-rich sulfide phases in EM1 (Table 4) may have been underrepresented in this section. Tungsten, which is also susceptible to oxidative loss but was not detected in the sulfides, is not depleted in this sample. Most of the Fremdlinge in Ef2 and Ef3 have flat normalized HSE abundances that vary by about a factor of 5 within each CAI (Figure 9). The patterns for each inclusion fall within an envelope defined by less than 5 K in condensation temperature (Figure 10B). This could represent either a narrowly restricted range of condensation temperatures of the metal, or slightly variable degrees of mixing of high-temperature metal condensates with low-temperature Fe-Ni alloy.

Any metal grains having condensation temperatures ≤ 1480 K should have HSE patterns that are flat through Re-Rh (Figure 10B), and could be diluted into metal with a lower condensation temperature to produce most of the refractory siderophile concentrations shown by the Fremdlinge in Efremovka. Fremdlinge HSE patterns could reflect either equilibrium with the nebula at a fixed temperature, or mixing of numerous precursor grains, each having a different condensation temperature. In either case most

Fremdlinge exhibit nearly chondritic HSE patterns, implying equilibrium with the nebular gas to $T_c \approx 1480$ K or below (Figure 10).

Some Fremdlinge, for example EM2 and EM13 in Ef2, do not have flat HSE patterns (Figure 9). These patterns, which are similar to some reported by Palme et al. (1994) for Fremdlinge in Allende, cannot be matched by condensation at a single temperature. For example, the Os/Pt fractionation in EM2, which is 3X chondritic, would require $T_c > 1500$ K (Figure 10), but at this temperature the abundances of the less refractory elements Ni, Co, Pd, and Fe should be several orders of magnitude lower than observed. Therefore, those Fremdlinge having gently sloping PGE abundance patterns are likely to represent mixtures of metal grains that condensed at various temperatures. Any PGE pattern that is flat or monotonically decreasing with increasing volatility of the elements can be matched by some mixture of alloys having different condensation temperatures. Because each component alloy must be removed from the nebula at the temperature T_c at which it last equilibrated with the gas, and the Fremdlinge are composed of a mixture of alloys having different T_c , the aggregation of alloys must have occurred within the CAIs and not prior to their incorporation into the inclusion. Similar conclusions were reached by Blum et al. (1989b), who suggested that many fine metal grains could have coalesced into larger proto-Fremdlinge during CAI formation, and by Sylvester et al. (1990; 1992; 1993), who modelled Fremdling formation as mixing of multiple alloys, each with separate condensation temperatures. Furthermore, since it is necessary for EM2 and other Fremdlinge with sloping PGE patterns to have formed by mixing of alloys with various T_c , it is probable that many or all Fremdlinge having flat PGE profiles formed in this way also.

Although most of the PGE patterns presented here are dominated by volatility effects, a few grains show fractionations between elements that are difficult to replicate with single-phase alloy condensation calculations, regardless of the mix of condensation temperatures. For example, EM19 in Ef2 has Ni, CI-normalized enrichments of ~60 for Os

and Ru, and ~100 for Ir, Pt, and Rh (Table 6). It is possible that these fractionations are the result of subsolidus phase exsolution between hcp (Os, Ru) and fcc (Ir, Pt, Rh) alloys, similar to the scenario presented by Blum et al. (1989b); this would imply that the laser ablation spot did not sample a portion that was representative of the bulk Fremdling. Alternatively, as suggested by Sylvester et al. (1990), it may indicate multiphase alloy condensation with later aggregation of multiple grains, having different crystal structures, to form the Fremdling.

Palme et al. (1994) measured several highly refractory-enriched Fremdlings in a single Allende CAI by electron microprobe and INAA; they observed variations in refractory element patterns that are similar to those shown in Figure 9, including both flat profiles that vary in abundance, and sloping patterns indicating volatile depletion like that of EM2 in Ef2 (Figure 9C). Palme et al. (1994) stated that these variations require that the Fremdlings formed prior to incorporation into the CAI, because metal segregation during melting of the CAI would be expected to produce uniform metal compositions. However, the expectation of uniform metal compositions assumes that either a) the Fremdlings were able to equilibrate with one another after metal segregation; or b) the Fremdlings aggregated from a large number of refractory-rich metal grains, such that all Fremdlings within an inclusion tended to the same mean compositions. As Palme et al. (1994) recognized, segregated PGE metal droplets in CAIs are not likely to equilibrate with one another. The solubility of highly siderophile elements in silicate melts is very low (Borisov and Palme, 2000), which would inhibit the diffusion between Fremdlings that is required for them to equilibrate without coalescing. Moreover, the amount of high-temperature condensate needed to enter the Fremdling could be very small relative to an FeNi alloy bearing chondritic proportions of HSEs. Although Palme et al. (1994) describe late addition of Fe and Ni to each Fremdling to match the observed composition, a more practical view is that a small amount of refractory-enriched metal is incorporated into what is primarily an FeNi alloy. For example, only ~1% of a 1480 K condensate needs to be mixed into an FeNi

alloy to produce the patterns observed in Ef2 Fremdlinge (Figure 9A); these condensate grains could be few in number and therefore not evenly mixed into the proto-Fremdlinge during CAI melting. In this way, Fremdlinge can form during melting and metal coalescence in a CAI (Blum et al., 1989b; Sylvester et al., 1990), while maintaining different refractory siderophile element enrichment patterns from one another. An even smaller high- T_c component is required when the condensation temperature is greater than 1500 K (Figure 10), as in the case of sloping PGE volatility patterns such as EM2 in Ef2 (Figure 9C). Therefore, it is not necessary that the Fremdlinge were assembled prior to incorporation into CAIs; it is only necessary that the refractory-enriched metal components that dominate the HSE patterns of Fremdlinge existed prior to entering CAIs.

Palme et al. (1994) also measured the HSE contents in chips from a few silicate "sockets" that had been adjacent to Fremdlinge, and found that the HSE abundances were similar to those of the bulk CAI (Egg 6 in Allende). Palme et al. (1994) stated that this is inconsistent with formation of Fremdlinge by coalescence of metal grains in a CAI, and they concluded from these analyses that the Fremdlinge represent an independent source of PGEs that is added to, rather than derived from, the bulk CAI. There are, however, two other possibilities. First, the ≥ 0.1 mg sockets that Palme et al. (1994) studied could have contained small Fremdlinge that were not observed. As discussed in Section 3.2 and shown in Ef2 in Figure 1, most Fremdlinge are $< 50 \mu\text{m}$ in size, much smaller than those studied by Palme et al. (1994). Second, it is possible that many of the refractory metal nuggets that Palme et al. (1994) consider to be the primary carrier of PGEs in CAIs are trapped inside of spinel grains that never dissolved in the CAI melt, and this protected the nuggets from absorption into the coalescing Fremdlinge. Indeed, all of the refractory nuggets that Eisenhour and Buseck (1992) identified as PGE metal condensates were found enclosed within spinel grains. In this scenario, the abundance of HSEs in the sockets would depend on the abundance of spinel grains and their refractory metal nugget inclusions.

4.3. Zoning of EM2

The rim of Fremdling EM2, in inclusion Ef2, is strongly depleted in W, Re, Os, Ir, and Pt, while unfractionated in Ru, Rh, and Pd, relative to the interior (Figure 8). This abundance pattern is similar to that which results from partitioning between schreibersite and metal phases, such as that observed in EM1 in Ef1 (Figure 5). Although there is no measurable phosphorus in the rim of EM2, the fractionation observed here between the heavy PGEs and the light PGEs is best explained through partitioning between the metallic interior of the Fremdling and a schreibersite layer occupying what is now the rim. The P in this postulated schreibersite could have been removed through later oxidation of the Fremdling, producing the outer phosphate layer now present (Figure 7) and leaving a metallic rim with inherited PGE signatures. The phosphate formation could have occurred at $f(\text{O}_2)$ well below the iron-wüstite buffer, as shown in Figure 11. The PGE pattern of EM18 in Ef2 (Figure 9A), which is similar to that of the EM2 rim (Figure 8) and the EM1 schreibersite (Figure 5), suggests that this Fremdling was also dominated by phosphide.

The identification of schreibersite as the precursor of the rim of EM2 places constraints on the history of this grain. The round shape and concentric compositional structure of the grain suggest that it crystallized from a molten metallic droplet. The inferred presence of schreibersite at the rim suggests either that schreibersite was the liquidus phase, with crystallization initiating on the outside of the droplet, or that subsolidus phosphide precipitation was promoted by nucleation at the surface of the grain. The phase diagram of the Fe-Ni-P system (Villars et al., 1995) shows that there is a small window of composition, approximately 17 to 23 at% P, in which schreibersite is on the liquidus. The low volume fraction of phosphide phantom in the rim of EM2 indicates that, if schreibersite were the liquidus phase, then the metal droplet composition was probably near the eutectic or a monovariant curve. This would allow only a small modal fraction (~10%) of

schreibersite to crystallize before the bulk of the droplet solidified into a metal+phosphide mixture, which survives as the core and mantle of the grain (Figure 6). If the original phosphides in EM2 formed exclusively below the solidus, then one might interpret the small grain size of the interior phosphides, relative to the massive band of phosphide phantom in the rim, as a result of different conditions for nucleation. In either scenario, during later, subsolidus oxidation, phosphorus diffused out of the rim schreibersite as well as from smaller phosphide grains and metal that occupied what is now the mantle of the grain. The boundary between the phosphide-bearing core and the phosphide-free mantle marks the point at which the local P concentration in the metal falls below the saturation level of P in the metal, due to diffusion of P through the Fremdling during oxidation. The Ca-phosphate that surrounds the Fremdling (Figure 7) was formed using P that left EM2 at this stage (Fisenko et al., 1992). The estimated amount of P contained in the Ca-phosphate rim in Figure 7A is less than the P inferred to be lost from the Fremdling. Depending on whether the schreibersite formed as the liquidus phase (high P) or as a subsolidus precipitate (low P), an additional ~2-4 times as much P is presumed to be present in the Fremdling but not revealed in the section studied.

4.4. Enrichment of Ni in Fremdlinge

All of the measured Ni contents in Fremdlinge in Ef2 are very high, between 45 and 83 wt% (Tables 5 and 6). Fremdlinge in Ef1 and Ef3 are also enriched in Ni, but to a lesser extent (Tables 3 and 6). These Ni/Fe ratios are much higher than those calculated to occur upon condensation from a solar gas (Grossman and Olsen, 1974), placing an important constraint on the history of the metal. The model presented above for formation of EM2 has significant implications for the question of Fe loss from Ef2 Fremdlinge.

The localized Fe enrichment documented by Fisenko et al. (1992) in the silicate of Ef2, surrounding the Fremdling EM2, suggests the possibility that Ni and other highly

siderophile elements were enriched in this sample by subsolidus diffusion of Fe from the Fremdling into the CAI. However, this is complicated by the phosphide/phosphate processing described above. Diffusion of P in Fe-Ni alloy is about 2 orders of magnitude faster than the Fe-Ni binary diffusion coefficient (Heyward and Goldstein, 1973), but EM2 shows a strong gradient in phosphide abundance and only a small gradient in Ni content (Table 5). This is the opposite of the expectation for P and Fe diffusion out of the grain during oxidation; with such a phosphide distribution, there should be a steep Ni gradient at the outer edge of the Fremdling, with the interior dominated by the original Ni content. A similar problem arises with respect to V, which diffuses faster than Fe-Ni binary diffusion by about an order of magnitude. There is a very steep V gradient at the rim/mantle interface in EM2 (Figure 7), and virtually no change in Ni content. If the Ni enrichment occurred by solid state diffusion of Fe into the surrounding inclusion, then the P and V gradients in EM2 should have been easily erased.

A mass balance of the Fe budget in Ef2 provides a second argument against the oxidative loss of Fe from EM2 into the bulk oxide portion of Ef2. Fisenko et al. (1992) provide modal estimates of melilite, pyroxene, spinel, and metal in the inclusion, as well as compositions of each phase. We calculate that the bulk silicate+oxide portion of Ef2 contains about 0.03 wt% Fe based on those data. The metal in Ef2 is dominated by EM2 due to its size, but all of the Fremdlings have very high Ni contents similar to the 54 wt% Ni in EM2 (Table 6). Assuming that the metal originally had <15 wt% Ni, which is the upper limit for a high-temperature condensate from a 10^{-3} bar solar nebula (Grossman and Olsen, 1974), then the Ef2 Fremdlinge must have lost ~80-90% of their original Fe. If all of this remained in the inclusion, then a mean silicate Fe content of ~3 wt% is required, which is two orders of magnitude higher than observed.

We conclude that Fe was lost from the metal at an early stage in CAI formation, prior to final solidification of the inclusion. This Fe loss may have taken place either prior to CAI agglomeration, possibly by partial, nonequilibrium evaporation of FeNi alloy into

an unsaturated gas, or during subsequent melting and evaporation of the CAI, when the diffusivity of Fe through the silicate melt would have been much higher than in the solid state. This early, high-temperature loss of Fe presumably occurred to Fremdlinge in the other CAIs, which show Ni enrichments that are substantial relative to the < 15 wt% expected in condensates, although less extreme than in Ef2.

4.5. Fractionations Between Refractory Siderophile Elements

4.5.1. Re/Os Ratios in Fremdlinge

Figure 12 shows the Re-Os data collected on Fremdlinge from Efremovka CAIs. Most of these Fremdlinge exhibit chondritic Re/Os ratios, as expected from calculated condensation sequences from a gas of solar composition. However, both Ef2 and Ef3 bear metal grains that have Re/Os ratios up to 2x chondritic values, with no correlation between Re/Os and Os abundance. Since Efremovka CAIs are among the least altered, with little evidence of significant post-CAI oxidation of the metal, the Re/Os variation can be considered to be inherited from heterogeneity among the metal grains that existed prior to assembly of the CAI. ^{187}Re decays to ^{187}Os with a half-life of 4.16×10^{10} yr (Smoliar et al., 1996). Becker et al. (2001) give a solar $^{187}\text{Re}/^{188}\text{Os}$ ratio of 0.3964, and a present value of $^{187}\text{Os}/^{188}\text{Os} = 0.1265$ for CAIs with solar Re/Os ratios, from which a range in present $^{187}\text{Os}/^{188}\text{Os}$ of 0.118-0.153 for bulk Fremdlinge in Ef2 and Ef3 can be calculated from the measured Re/Os ratios. A single Fremdling from Ef2 has Re/Os of 0.5xCI and an Os abundance of 4880 ppm, and is excluded from the range. The calculated $^{187}\text{Os}/^{188}\text{Os}$ range for Fremdlinge in Ef2 and Ef3 is a factor of 7 larger than that of the bulk CAI data of Becker et al. (2001), which exhibit a range of 0.125-0.130 (exclusive of Group II CAIs), implying that bulk CAIs averaged the contributions from numerous Fremdlinge to approach the solar Re/Os value.

4.5.2. Oxidation of Mo and W

There are negative W and Mo anomalies of varying magnitude in many Fremdlinge (Figures 3 and 9); these have been observed previously in Fremdlinge in Allende and were ascribed to late-stage oxidation and migration of W and Mo into the silicate host (Palme et al., 1994). Bulk INAA data from the Ef3 CAI (Sylvester et al., 1993) are compared in Figure 3 to the LA-ICP-MS data for The Heart in Ef3; the pattern for Re and the PGEs in bulk Ef3 is similar to the analyses of the Heart. The bulk inclusion shows a much smaller depletion of W and Mo than the Fremdling, which is consistent with the observations of Palme et al. (1994). Vanadium is also enriched in the bulk inclusion relative to the Fremdling, suggesting that, like W and Mo, V resides primarily in the silicate host. These elements could have entered the silicate phase either during condensation or by later redistribution from the Fremdlinge.

Condensation of Mo and W as trace constituents in a silicate or oxide, either molten or solid, has not been considered even in the most recent and comprehensive calculations (e.g., Ebel and Grossman, 2000). Davis et al. (1982) calculated that the solid/gas partition coefficient for V at 1723 K was lower at the IW buffer than under solar nebula conditions ($\Delta IW \approx -6$) by a factor of about 1000. Simon et al. (2001) reported V in hibonite, a mineral that condenses very early in the condensation sequence, and concluded that this V was primary, reflecting condensation at low $f(O_2)$.

Figure 9B shows that other Fremdlinge in Ef3 show a variety of Mo and W anomalies; some Fremdlinge are undepleted in these elements, while others are depleted by over an order of magnitude relative to the PGEs. Likewise, the Fremdlinge in Ef2 also have Mo and W anomalies of varying magnitude. These variations could be a result of varying oxygen fugacities prior to incorporation of the Fremdlinge into the CAIs; differences in $f(O_2)$ would cause V, Mo, and W to enter coexisting silicate or gaseous oxide phases to varying degrees. Fegley and Palme (1985) calculated that depletions due to gaseous W- and

Mo-oxide formation in an oxidizing nebula were always smaller for W than for Mo. Nearly all of the Fremdlinge studied here satisfy this constraint. However, this model requires that Fremdlinge within a single CAI record large variations in nebular $f(\text{O}_2)$.

An alternative is that V, Mo, and W were redistributed into the silicate portion of the inclusion by a later oxidizing event. The INAA data on the bulk Ef3 inclusion (Sylvester et al., 1993) (Figure 3), that indicate that significant V, Mo, and W reside in the silicate portion of the inclusion, are consistent with this scenario. Palme et al. (1994) similarly concluded that much of the W originally residing in Fremdlinge in Allende CAIs was later mobilized into the surrounding silicate during low-temperature oxidation. A difficulty with this model for Efremovka CAIs is that, as discussed above in the case of Ef2, there is little Fe in the silicate inclusion; any event that oxidized the siderophiles Mo and W should have oxidized some Fe as well.

5. CONCLUSIONS

Secondary sulfidation of CAIs in members of the oxidized subgroup of CV3 chondrites may have significantly altered the distribution of PGEs and other siderophile elements in the Fremdlinge, as documented by the measured PGE abundances in a sulfide vein in CAI TS68 from Allende. In particular, late-stage sulfidation may have been responsible for disturbing the Re/Os ratios in refractory inclusions in Allende. Geochemical investigations targeting the early stages of metal formation in CAIs should focus on the reduced CV3 subgroup.

Siderophile element microdistributions in Fremdlinge in Efremovka suggest the following stages of formation: 1) Condensation of metal at a range of temperatures, predominantly below ~ 1480 K. Some HSE fractionations in individual Fremdlinge, including Re/Os ratios and possibly W and Mo anomalies, may have occurred prior to CAI formation. 2) Incorporation of metal grains into CAIs. Iron loss, leading to Ni

enhancement, may have occurred prior to incorporation or during subsequent melting. 3) Melting of CAIs led to coalescence of metal and caused Fremdlinge to be rounded. In some, if not all, cases, incomplete mixing of high- T_c and low- T_c metal produced variably enriched Fremdlinge with flat HSE patterns, as well as Fremdlinge with sloping, volatility-controlled HSE patterns. The Fremdlinge did not equilibrate with one another because of the low solubility of HSEs in silicate. 4) Subsolidus precipitation of oxides, phosphides, and minor sulfides occurs at low temperatures. Also oxidation, even at low $f(O_2)$ (well below the iron-wüstite buffer), can convert schreibersite to P-poor metal + phosphate.

The presence of distinct HSE patterns in Fremdlinge from a single CAI indicates that the study of individual Fremdlinge provides greater insights into the nature of refractory precursors to CAIs than do studies of bulk CAIs. Variable Re/Os ratios between individual Fremdlinge were probably established prior to CAI formation and inherited by some bulk CAIs. Precise dating of individual Efremovka Fremdlinge would better constrain nebular chronology.

Acknowledgments—We are grateful to A. Fisenko for providing specimens of Efremovka. Discussions with D. Ebel and A. Davis were beneficial. Helpful reviews were provided by H. Becker, A. El Goresy, and an anonymous reviewer. This work was supported by NASA through grants NAG 5-9800 to M. H. and NAG 5-4476 to L. G.

REFERENCES

- Anders E. and Grevesse N. (1989) Abundances of the elements: Meteoritic and solar. *Geochim. Cosmochim. Acta* **53**, 197-214.
- Barin I. (1995) *Thermochemical Data of Pure Substances*, VCH, Weinheim, Germany.
- Becker H., Morgan J. W., Walker R. J., MacPherson G. J. and Grossman J. N. (2001) Rhenium-Osmium systematics of calcium-aluminum-rich inclusions in carbonaceous chondrites. *Geochim. Cosmochim. Acta* **65**, 3379-3390.
- Bischoff A. and Palme H. (1987) Composition and mineralogy of refractory-metal-rich assemblages from a Ca,Al-rich inclusion in the Allende meteorite. *Geochim. Cosmochim. Acta* **51**, 2733-2748.
- Blander M., Fuchs L. H., Horowitz C. and Land R. (1980) Primordial refractory metal particles in the Allende meteorite. *Geochim. Cosmochim. Acta* **44**, 217-223.
- Blum J. D., Wasserburg G. J., Hutcheon I. D., Beckett J. R. and Stolper E. M. (1988) 'Domestic' origin of opaque assemblages in refractory inclusions in meteorites. *Nature* **331**, 405-409.
- Blum J. D., Wasserburg G. J., Hutcheon I. D., Beckett J. R. and Stolper E. M. (1989a) Diffusion, phase equilibria and partitioning experiments in the Ni-Fe-Ru system. *Geochim. Cosmochim. Acta* **53**, 483-489.
- Blum J. D., Wasserburg G. J., Hutcheon I. D., Beckett J. R. and Stolper E. M. (1989b) Origin of opaque assemblages in C3V meteorites: Implications for nebular and planetary processes. *Geochim. Cosmochim. Acta* **53**, 543-556.
- Borisov A. and Palme H. (2000) Solubilities of noble metals in Fe-containing silicate melts as derived from experiments in Fe-free systems. *Am. Mineral.* **85**, 1665-1673.
- Buchwald V. F. (1975) *Handbook of Iron Meteorites*. Univ. California Press, Berkeley.
- Campbell A. J. and Humayun M. (1999a) Trace element microanalysis in iron meteorites by laser ablation ICPMS. *Anal. Chem.* **71**, 939-946.

- Campbell A. J. and Humayun M. (1999b) Microanalysis of platinum group elements in iron meteorites using laser ablation ICP-MS. *Lunar Planet. Sci. XXX*. Lunar Planet. Inst., Houston. #1974 (abstr.).
- Campbell A. J., Simon S. B., Humayun M. and Grossman L. (1999) Microanalysis of siderophile elements in Fremdlinge using laser ablation ICP-MS. *Lunar Planet. Sci. XXX*. Lunar Planet. Inst., Houston. #1609 (abstr.).
- Campbell A. J., Humayun M. and Weisberg M. K. (2001a) Siderophile element constraints on the formation of metal in the metal-rich chondrites Bencubbin, Weatherford, and Gujba. *Geochim. Cosmochim. Acta*, in press.
- Campbell A. J., Humayun M., Meibom A., Krot A. N. and Keil K. (2001b) Origin of zoned metal grains in the QUE94411 chondrite. *Geochim. Cosmochim. Acta* **65**, 163-180.
- Casanova I. and Grossman L. (1993) Distribution of vanadium and melting of opaque assemblages in Efremovka CAIs. *Lunar Planet. Sci. XXIV*, 257-258.
- Chase M. W. Jr. (1998) *NIST-JANAF Thermochemical Tables*, 4th ed. *J. Phys. Chem. Ref. Data* Monograph No. 9, American Institute of Physics.
- Clayton R. N., Grossman L. and Mayeda T. K. (1973) A component of primitive nuclear composition in carbonaceous meteorites. *Science* **182**, 485-488.
- Clayton R. N., Onuma N., Grossman L. and Mayeda T. K. (1977) Distribution of the presolar component in Allende and other carbonaceous chondrites. *Earth Plan. Sci. Lett.* **34**, 209-224.
- Clayton R. N., Mayeda T. K. and Epstein S. (1978) Isotopic fractionation of silicon in Allende inclusions. *Proc. Lunar Planet. Sci. Conf.* **9**, 1267-1278.
- Clayton R. N., Mayeda T. K. and Molini-Velsko C. A. (1985) Isotopic variations in solar system material: evaporation and condensation of silicates. In *Protostars and Planets II* (eds. D. C. Black and M. S. Matthews), pp. 755-771. Univ. Arizona Press.

- Clayton R. N., Hinton R. W. and Davis A. M. (1988) Isotopic variations in the rock-forming elements in meteorites. *Phil. Trans. Roy. Soc. A* **325**, 483-501.
- Davis A. M. and Grossman L. (1979) Condensation and fractionation of rare earths in the solar nebula. *Geochim. Cosmochim. Acta* **43**, 1611-1632.
- Davis A. M., Tanaka T., Grossman L., Lee T. and Wasserburg G. J. (1982) Chemical composition of HAL, an isotopically-unusual Allende inclusion. *Geochim. Cosmochim. Acta* **46**, 1627-1651.
- Ebel D. and Grossman L. (2000) Condensation in dust-enriched systems. *Geochim. Cosmochim. Acta*, **64**, 339-366.
- Eisenhour D. D. and Buseck P. R. (1992) Transmission electron microscopy of RMNs: Implications for single-phase condensation of the refractory siderophile elements. *Meteoritics* **27**, 217-218.
- El Goresy A., Nagel K. and Ramdohr P. (1978) Fremdlinge and their noble relatives. *Proc. Lunar Planet. Sci. Conf. 9th*, 1279-1303.
- Fegley B. Jr. and Palme H. (1985) Evidence for oxidizing conditions in the solar nebula from Mo and W depletions in refractory inclusions in carbonaceous chondrites. *Earth Plan. Sci. Lett.* **72**, 311-326.
- Fisenko A. V., Ignatenko K. I. and Lavrukhina A. K. (1992) The metallic phase in a Type B1 CAI fragment in the Yefremovka CV chondrite. *Geochem. Int.* **29**, 85-93.
- Grossman L. (1972) Condensation in the primitive solar nebula. *Geochim. Cosmochim. Acta* **36**, 597-619.
- Grossman L. (1980) Refractory inclusions in the Allende meteorite. *Ann. Rev. Earth Planet. Sci.* **8**, 559-608.
- Grossman L. and Olsen E. (1974) Origin of the high-temperature fraction of C2 chondrites. *Geochim. Cosmochim. Acta* **38**, 173-187.
- Grossman L., Ebel D. S., Simon S. B., Davis A. M., Richter F. M. and Parsad N. M. (2000) Major element chemical and isotopic compositions in refractory inclusions in C3

- chondrites: The separate roles of condensation and evaporation. *Geochim. Cosmochim. Acta* **64**, 2879-2894.
- Grossman L., Ebel D. S., and Simon S. B. (2001) Formation of refractory inclusions by evaporation of condensate precursors. *Geochim. Cosmochim. Acta*, in press.
- Heyward T. R. and Goldstein J. I. (1973) Ternary diffusion in the α and γ phases of the Fe-Ni-P system. *Metall. Trans.* **4**, 2335-2342.
- Horan M. F., Walker R. J. and Rubin A. E. (2001) Highly siderophile elements in shocked and unshocked chondrites. *Lunar Planet. Sci. XXXII*. Lunar Planet. Inst., Houston. #1577 (abstr.).
- Hultgren R., Desai P. D., Hawkins D. T., Gleiser M., Kelley K. K. and Wagman D. D. (1973) *Selected Values of the Thermodynamic Properties of the Elements*, American Society for Metals.
- Hutcheon I. D., Armstrong J. T. and Wasserburg G. J. (1987) Isotopic studies of Mg, Fe, Mo, Ru and W in Fremdlinge from Allende refractory inclusions. *Geochim. Cosmochim. Acta* **51**, 3175-3192.
- Knacke O., Kubaschewski O. and Hesselmann K. (1991) *Thermochemical Properties of Inorganic Substances*, Springer-Verlag, Berlin.
- MacPherson G. J., Wark D. A., and Armstrong J. T. (1988) Primitive material surviving in chondrites: Refractory inclusions. In *Meteorites and the Early Solar System* (eds. J. F. Kerridge and M. S. Matthews), pp. 746-807. Univ. Arizona Press.
- McSween H. Y. Jr. (1977) Petrographic variations among carbonaceous chondrites of the Vigarano type. *Geochim. Cosmochim. Acta* **41**, 1777-1790.
- Palme H. and Wlotzka F. (1976) A metal particle from a Ca,Al-rich inclusion from the meteorite Allende, and the condensation of refractory siderophile elements. *Earth Plan. Sci. Lett.* **33**, 45-60.

- Palme H., Hutcheon I. D. and Spettel B. (1994) Composition and origin of refractory-metal-rich assemblates in a CaAl-rich Allende inclusion. *Geochim. Cosmochim. Acta* **58**, 495-513.
- Podosek F. A., Zinner E. K., MacPherson G. J., Lundberg L. L., Brannon J. C. and Fahey A. J. (1991) Correlated study of initial Sr-87/Sr-86 and Al-Mg isotopic systematics and petrologic properties in a suite of refractory inclusions from the Allende meteorite. *Geochim. Cosmochim. Acta* **55**, 1085-1110.
- Schmitt W., Palme H. and Wänke H. (1989) Experimental determination of metal/silicate partition coefficients for P, Co, Ni, Cu, Ga, Ge, Mo, and W and some implications for the early evolution of the Earth. *Geochim. Cosmochim. Acta* **53**, 173-185.
- Simon S. B., Davis A. M. and Grossman L. (1999) Origin of compact type A refractory inclusions from CV3 carbonaceous chondrites. *Geochim. Cosmochim. Acta* **63**, 1233-1248.
- Simon S. B., Davis A. M. and Grossman L. (2001) Formation of orange hibonite, as inferred from some Allende inclusions. *Meteorit. Planet. Sci.* **36**, 331-350.
- Smoliar M. I., Walker R. J. and Morgan J. W. (1996) Re-Os ages of group IIA, IIIA, IVA, and IVB iron meteorites. *Science* **271**, 1099-1102.
- Sylvester P. J., Ward B. J., Grossman L. and Hutcheon I. D. (1990) Chemical compositions of siderophile element-rich opaque assemblates in an Allende inclusion. *Geochim. Cosmochim. Acta* **54**, 3491-3508.
- Sylvester P. J., Simon S. B. and Grossman L. (1992) Chemical compositions of Fremdlinge from a type A Allende inclusion. *Lunar Planet. Sci.* **XXIII**, 1397-1398.
- Sylvester P. J., Simon S. B. and Grossman L. (1993) Refractory inclusions from the Leoville, Efremovka, and Vigarano C3V chondrites: Major element differences between Types A and B, and extraordinary refractory siderophile element composition. *Geochim. Cosmochim. Acta* **57**, 3763-3784.

- Villars P., Prince A. and Okamoto H. (1995) *Handbook of Ternary Alloy Phase Diagrams*, ASM International.
- Walker R. J., Horan M. F., Morgan J. W. and Meisel T. (2001) Osmium isotopic compositions of chondrites and Earth's primitive upper mantle: constraints on the late veneer. *Lunar Planet. Sci. XXXII*. Lunar Planet. Inst., Houston. #1152 (abstr.).
- Wang J., Davis A. M., Clayton R. N., Mayeda T. K. and Hashimoto A. (2001) Chemical and isotopic fractionation during the evaporation of the FeO-MgO-SiO₂-CaO-Al₂O₃-TiO₂ rare earth element melt system. *Geochim. Cosmochim. Acta* **65**, 479-494.
- Wark D. A. (1986) Evidence for successive episodes of condensation at high temperature in a part of the solar nebula. *Earth Planet. Sci. Lett.* **77**, 129-148.
- Wasserburg G. J., Lee T. and Papanastassiou D. A. (1977) Correlated O and Mg isotopic anomalies in Allende inclusions. 2. Magnesium. *Geophys. Res. Lett.* **4**, 299-302.
- Weisberg M. K., Prinz M., Clayton R. N. and Mayeda T. K. (1997) CV3 chondrites: Three subgroups, not two. *Meteorit. Planet. Sci.* **32**, A138-A139.

TABLES

Table 1. Composition of sulfide vein in the Allende CAI, TS68. Italics denote detection limits.

X	Abundance	X/CI
S	33.5 wt%	5.4
V	0.03	4.7
Fe	44.6	2.3
Co	1.0	20.9
Ni	20.6	18.8
Mo	63.1 ppm	68.0
Ru	1136.5	1596.2
Rh	35.4	264.3
Pd	2.8	5.0
W	29.8	322.3
Re	<i>0.3</i>	8.2
Os	2.1	4.4
Ir	<i>0.1</i>	<i>0.2</i>
Pt	<i>0.5</i>	<i>0.5</i>
Au	<i>0.6</i>	<i>4.2</i>

Table 2. LA-ICP-MS abundance data from the Heart, a Fremdling in Efremovka CAI Ef3. All values are in mg/g. Italics indicate detection limits. Errors are 2σ .

	V	Fe	Co	Ni	Mo	Ru	Rh
#1	4.3 ± 0.5	830 ± 9	9.0 ± 0.5	161 ± 8	<i>0.07</i>	0.68 ± 0.08	0.28 ± 0.03
#2	3.1 ± 0.3	761 ± 13	5.4 ± 0.3	233 ± 12	<i>0.05</i>	0.84 ± 0.10	0.24 ± 0.03
#3	7.6 ± 0.8	915 ± 5	8.3 ± 0.4	77 ± 4	0.15 ± 0.03	0.69 ± 0.08	0.26 ± 0.03
#4	2.6 ± 0.3	774 ± 12	6.8 ± 0.3	219 ± 11	<i>0.05</i>	0.84 ± 0.10	0.23 ± 0.03
#5	3.9 ± 0.4	686 ± 16	6.1 ± 0.3	307 ± 15	<i>0.05</i>	0.66 ± 0.08	0.26 ± 0.03
average	4.3 ± 1.8	793 ± 76	7 ± 1	200 ± 77	<i>0.1</i>	0.74 ± 0.08	0.25 ± 0.02
	Pd	W	Re	Os	Ir	Pt	
#1	<i>0.03</i>	0.0010 ± 0.0009	0.048 ± 0.006	0.40 ± 0.05	0.39 ± 0.04	1.26 ± 0.14	
#2	<i>0.02</i>	0.0421 ± 0.0058	0.034 ± 0.005	0.44 ± 0.05	0.33 ± 0.04	0.78 ± 0.09	
#3	<i>0.03</i>	0.0026 ± 0.0011	0.041 ± 0.005	0.45 ± 0.05	0.39 ± 0.04	0.96 ± 0.11	
#4	<i>0.02</i>	0.0015 ± 0.0009	0.024 ± 0.004	0.41 ± 0.05	0.33 ± 0.04	1.12 ± 0.13	
#5	<i>0.02</i>	0.0016 ± 0.0008	0.025 ± 0.004	0.37 ± 0.04	0.39 ± 0.04	1.14 ± 0.13	
average	<i>0.02</i>	0.0098 ± 0.0027	0.034 ± 0.009	0.42 ± 0.03	0.37 ± 0.03	1.05 ± 0.17	

Table 3. LA-ICP-MS abundance data from EM1, a Fremdling in Efremovka CAI Ef1. All values are in mg/g. Italics indicate detection limits. Errors are 2σ .

	P	V	Fe	Co	Ni	Mo	Ru	Rh
phosphide	109±16	0.1 ± 0.1	320±68	1.5 ± 0.5	570 ± 53	0.05±0.02	0.16 ± 0.04	0.030 ± 0.004
kamacite	2	0.8 ± 1.3	914±33	23.5 ± 2.6	63 ± 11	0.02±	0.10 ± 0.06	0.035 ± 0.015
taenite	0.5	1.6 ± 0.3	672±78	5.6 ± 2.1	322 ± 80	0.12±0.18	0.12 ± 0.03	0.032 ± 0.005
V-sulfide	0.5	6.4 ± 1.0	669±118	9.4 ± 8.1	321 ± 126	1.93±1.27	0.14 ± 0.01	0.036 ± 0.016
bulk	8.1±1.2	1.2 ± 0.6	742±41	12.8 ± 1.5	228 ± 40	0.09±0.09	0.12 ± 0.03	0.033 ± 0.007
	Pd	W	Re	Os	Ir	Pt	Au	
phosphide	0.008	0.009	0.0002	0.0003	0.0001	0.003	0.001	
kamacite	0.007	0.023±0.007	0.009±0.005	0.08±0.03	0.08±0.02	0.16±0.06	0.002	
taenite	0.015±0.009	0.015±0.003	0.006±0.004	0.10±0.03	0.08±0.01	0.15±0.03	0.001	
V-sulfide	0.010±0.004	0.022±0.006	0.007±0.002	0.10±0.01	0.09±0.02	0.19±0.02	0.001	
bulk	0.009±0.004	0.017±0.003	0.007±0.003	0.09±0.02	0.074±0.011	0.14±0.03	0.001	

Table 4. Electron microprobe analyses of sulfides in EM1 in Efremovka CAI Ef1.

#	S	V	Fe	Mo	sum
wt%:					
1	41.390	34.151	10.244	12.961	98.746
2	42.384	35.858	10.438	11.573	100.253
5	37.457	11.585	48.396	0.324	97.762
6	41.710	33.497	10.944	13.436	99.587
8	38.667	15.945	43.862	0.404	98.878
9	39.227	16.450	40.722	4.384	100.783
atoms / 4 S:					
1	4.000	2.078	0.568	0.419	3.065
2	4.000	2.130	0.566	0.365	3.061
5	4.000	0.779	2.967	0.012	3.758
6	4.000	2.022	0.603	0.431	3.055
8	4.000	1.038	2.605	0.014	3.658
9	4.000	1.056	2.384	0.149	3.590

Table 5. LA-ICP-MS data from EM2, a Fremdling in Efremovka CAI Ef2. All values are in mg/g. Italics indicate detection limits. Errors are 2σ .

	P	V	Fe	Co	Ni	Mo	Ru	Rh
rim	<i>0.5</i>	0.15 ± 0.02	438 ± 22	17.3 ± 0.9	545 ± 27	0.20 ± 0.03	1.2 ± 0.1	0.18 ± 0.02
rim	<i>0.5</i>	0.70 ± 0.08	457 ± 23	16.1 ± 0.8	528 ± 26	0.09 ± 0.02	1.1 ± 0.1	0.16 ± 0.02
rim	0.7 ± 0.5	0.10 ± 0.02	466 ± 24	25.7 ± 1.3	507 ± 25	0.07 ± 0.02	1.3 ± 0.2	0.19 ± 0.02
mantle	<i>0.5</i>	4.92 ± 0.54	457 ± 23	17.1 ± 0.9	526 ± 26	1.25 ± 0.15	1.0 ± 0.1	0.15 ± 0.02
mantle	<i>0.5</i>	5.93 ± 0.65	401 ± 20	21.1 ± 1.1	578 ± 29	1.46 ± 0.17	1.2 ± 0.1	0.16 ± 0.02
mantle	<i>0.5</i>	5.08 ± 0.56	436 ± 22	19.2 ± 1.0	546 ± 27	1.59 ± 0.18	1.2 ± 0.1	0.19 ± 0.02
core	9.9 ± 1.2	4.89 ± 0.54	413 ± 21	15.7 ± 0.8	562 ± 28	4.64 ± 0.52	1.4 ± 0.2	0.18 ± 0.02
core	9.4 ± 1.1	5.19 ± 0.57	402 ± 20	19.0 ± 1.0	569 ± 28	2.15 ± 0.24	1.5 ± 0.2	0.18 ± 0.02
bulk	3.8 ± 0.2	4.7 ± 0.4	425 ± 18	18.5 ± 1.8	553 ± 17	2.0 ± 0.9	1.25 ± 0.07	0.171 ± 0.014

	Pd	W	Re	Os	Ir	Pt	Au
rim	0.02 ± 0.01	0.04 ± 0.01	0.026 ± 0.004	0.26 ± 0.03	0.19 ± 0.02	0.27 ± 0.03	<i>0.002</i>
rim	0.03 ± 0.01	0.05 ± 0.01	0.053 ± 0.007	0.75 ± 0.08	0.52 ± 0.06	0.56 ± 0.06	<i>0.002</i>
rim	0.04 ± 0.01	0.06 ± 0.01	0.007 ± 0.002	0.04 ± 0.01	0.02 ± 0.00	0.13 ± 0.02	<i>0.003</i>
mantle	0.03 ± 0.01	0.20 ± 0.02	0.126 ± 0.015	1.52 ± 0.17	1.15 ± 0.13	1.09 ± 0.12	<i>0.002</i>
mantle	0.02 ± 0.01	0.16 ± 0.02	0.141 ± 0.017	1.90 ± 0.21	1.16 ± 0.13	1.16 ± 0.13	<i>0.003</i>
mantle	0.03 ± 0.01	0.21 ± 0.02	0.141 ± 0.017	1.76 ± 0.19	1.35 ± 0.15	1.20 ± 0.14	<i>0.003</i>
core	0.03 ± 0.01	0.34 ± 0.04	0.170 ± 0.020	1.70 ± 0.19	1.24 ± 0.14	1.00 ± 0.11	<i>0.003</i>
core	0.03 ± 0.01	0.25 ± 0.03	0.151 ± 0.018	1.55 ± 0.17	1.17 ± 0.13	1.07 ± 0.12	<i>0.002</i>
bulk	0.028 ± 0.004	0.21 ± 0.04	0.134 ± 0.009	1.55 ± 0.14	1.12 ± 0.08	1.03 ± 0.05	<i>0.002</i>

Table 6. LA-ICP-MS abundance data from Fremdlinge in Efremovka CAIs Ef2 and Ef3. All values are in mg/g. Italics indicate detection limits. Errors are 2σ .

	V	Fe	Co	Ni	Mo	Ru	Rh
Ef2:							
EM1	6.2±0.7	308 ± 34	18.0±0.9	674±34	5.5±0.6	2.7±0.3	0.8±0.1
EM7	3.1±0.3	392 ± 29	21.7±1.1	586±29	0.1±0.0	2.4±0.3	0.7±0.1
EM10	9.1±1.0	311 ± 34	13.6±0.8	675±34	0.1±0.1	2.8±0.3	0.7±0.1
EM10	5.1±0.6	492 ± 25	18.4±1.0	489±25	0.2±0.1	2.1±0.3	0.6±0.1
EM11	4.5±0.5	170 ± 42	11.9±1.1	819±42	8.9±1.1	6.0±0.8	1.1±0.2
EM12	14.5±1.8	142 ± 48	31.3±3.4	827±48	7.7±1.3	8.1±1.4	1.1±0.3
EM13	174±21	298 ± 127	138±14	588±127	9.6±4.4	14.9±5.1	3.2
EM14	5.7±0.7	272 ± 37	29.4±1.9	693±37	4.7±0.7	3.6±0.6	0.9±0.2
EM15	7.3±0.8	403 ± 29	19.2±1.0	567±29	0.5±0.1	5.0±0.6	0.9±0.1
EM16	2.7±0.3	526 ± 23	17.1±1.0	453±23	0.3±0.1	1.9±0.3	0.4±0.1
EM17	3.5±0.4	252 ± 37	24.7±1.4	726±37	2.4±0.4	4.4±0.6	0.8±0.1
EM18	9.8±1.1	179 ± 38	18.8±1.1	739±38	0.8±0.2	6.8±0.9	1.0±0.2
EM19	11.4±1.3	374 ± 33	13.9±1.2	612±33	0.6±0.3	2.4±0.5	0.8±0.2
Ef3:							
EM12	2.0±0.2	805 ± 10	10.4±0.6	184±9	2.5±0.3	3.1±0.4	0.8±0.1
EM13	2.4±0.3	812 ± 9	8.8±0.5	169±9	1.4±0.2	1.7±0.2	0.6±0.1
EM15	10.6±1.6	666 ± 27	5.2±1.7	308±27	<i>0.4</i>	0.5±0.4	<i>0.2</i>
EM16	8.4±1.0	858 ± 9	8.4±0.6	138±8	1.3±0.2	2.6±0.4	0.6±0.1
EM23	6.3±0.9	719 ± 18	15.7±1.3	265±18	2.2±0.5	2.6±0.5	1.4±0.2
EM24	3.7±0.4	666 ± 17	6.6±0.4	328±17	0.1±0.1	6.2±0.7	0.6±0.1
EM34	4.8±0.9	750 ± 21	14.5±1.7	236±21	2.1±0.6	7.5±1.2	0.9±0.2
EM35	9.4±1.1	744 ± 15	11.9±1.0	244±15	0.5±0.2	4.0±0.6	1.7±0.2
EM36	2.7±0.3	867 ± 7	6.5±0.4	128±7	0.5±0.1	1.7±0.2	0.8±0.1
EM37	5.6±0.6	872 ± 6	7.9±0.4	120±6	3.5±0.4	2.2±0.3	0.7±0.1
EM38	0.9±0.1	834 ± 8	11.1±0.6	159±8	0.0±0.0	1.6±0.2	0.8±0.1
	Pd	W	Re	Os	Ir	Pt	Au
Ef2:							
EM1	0.07±0.01	0.27±0.03	0.11±0.01	1.5±0.2	1.5±0.2	3.5±0.4	<i>0.002</i>
EM7	0.04±0.01	0.38±0.04	0.15±0.02	1.8±0.2	1.7±0.2	3.4±0.4	<i>0.002</i>
EM10	0.11±0.05	0.23±0.03	0.22±0.03	1.8±0.2	2.0±0.2	2.7±0.3	<i>0.016</i>
EM10	0.06±0.03	0.51±0.06	0.16±0.02	2.0±0.2	1.6±0.2	3.1±0.4	<i>0.013</i>
EM11	<i>0.15</i>	0.35±0.06	0.21±0.04	4.9±0.6	4.2±0.5	7.1±0.8	<i>0.050</i>
EM12	<i>0.53</i>	1.08±0.20	0.45±0.10	3.3±0.4	5.6±0.7	4.8±0.7	<i>0.173</i>
EM13	<i>2.04</i>	6.78±1.48	1.49±0.52	18.5±2.8	10.8±1.7	5.8±1.7	<i>1.141</i>
EM14	<i>0.18</i>	0.64±0.11	0.21±0.05	2.5±0.3	2.5±0.3	3.0±0.4	<i>0.099</i>
EM15	0.07±0.06	0.20±0.03	0.42±0.05	3.6±0.4	3.9±0.4	4.6±0.5	<i>0.026</i>
EM16	<i>0.05</i>	0.13±0.03	0.04±0.01	0.7±0.1	0.9±0.1	1.6±0.2	<i>0.030</i>
EM17	<i>0.08</i>	0.44±0.07	0.22±0.04	2.6±0.3	3.8±0.4	3.8±0.5	<i>0.046</i>
EM18	<i>0.09</i>	0.04±0.02	0.03±0.01	0.1±0.0	0.1±0.0	0.1±0.0	<i>0.049</i>
EM19	<i>0.15</i>	0.24±0.06	0.25±0.05	1.6±0.2	2.6±0.3	5.7±0.7	<i>0.086</i>
Ef3:							
EM12	<i>0.05</i>	0.18±0.03	0.12±0.02	1.2±0.1	1.3±0.2	3.7±0.4	<i>0.016</i>
EM13	<i>0.01</i>	0.16±0.02	0.10±0.01	0.7±0.1	0.9±0.1	3.1±0.3	<i>0.007</i>
EM15	<i>0.29</i>	0.03±0.05	0.04±0.04	0.2±0.1	0.5±0.1	1.2±0.3	<i>0.144</i>
EM16	<i>0.06</i>	0.14±0.03	0.11±0.02	1.5±0.2	0.8±0.1	2.2±0.3	<i>0.029</i>
EM23	<i>0.39</i>	0.35±0.09	0.19±0.05	2.7±0.3	2.6±0.3	5.0±0.6	<i>0.136</i>
EM24	<i>0.08</i>	0.03±0.01	0.27±0.04	3.0±0.3	3.6±0.4	3.8±0.4	<i>0.027</i>
EM34	<i>0.56</i>	0.14±0.08	0.26±0.07	3.4±0.5	5.9±0.7	7.5±1.0	<i>0.195</i>
EM35	<i>0.27</i>	0.34±0.08	0.25±0.05	1.8±0.2	2.2±0.3	6.5±0.8	<i>0.093</i>
EM36	<i>0.01</i>	0.11±0.02	0.10±0.01	1.0±0.1	1.1±0.1	2.8±0.3	<i>0.006</i>
EM37	<i>0.05</i>	0.08±0.02	0.09±0.01	1.1±0.1	1.1±0.1	4.3±0.5	<i>0.018</i>
EM38	<i>0.01</i>	0.01±0.00	0.12±0.02	0.9±0.1	1.2±0.1	3.1±0.4	<i>0.007</i>

FIGURE CAPTIONS

Figure 1. Backscattered electron image of the Efremovka CAI Ef2. mel = melilite; sp = spinel; met = metal. The large metal object at the bottom is the Fremdling EM2.

Figure 2. Backscattered electron image of the Heart, a Fremdling in Efremovka CAI Ef3. Light gray: taenite; medium gray: kamacite; black grains: vanadium-rich magnetite. A phosphate vein, also black, is indicated. Circles show locations of LA-ICP-MS analyses. Scale bar = 50 μm .

Figure 3. Siderophile element concentrations in an Efremovka CAI, Ef3. Squares: LA-ICP-MS analyses of numbered points from the Heart, a single Fremdling; circles: bulk values for Ef3 by INAA (Sylvester et al., 1993). In this and subsequent figures, concentrations are normalized to Ni and CI chondrites (Anders and Grevesse, 1989) and the elements are listed in order of increasing volatility in the solar nebula. Data below detection limits ($\sim 2\times\text{CI}$ for Pd/Ni, $\sim 4\times\text{CI}$ for Mo/Ni) are omitted.

Figure 4. Backscattered electron image of EM1, a Fremdling in Efremovka CAI Ef1. Light gray: taenite (tae); medium gray: schreibersite (sch); dark gray: kamacite (kam); black grains: vanadium-rich sulfide (V). Circles show locations of LA-ICP-MS analyses. Scale bar = 100 μm .

Figure 5. Siderophile element concentrations in different phases in Fremdling EM1, measured by LA-ICP-MS. Each pattern represents an average of two measurements of that phase. Downward arrows indicate upper bounds (measurement below detection limits).

Figure 6. Backscattered electron image of EM2, a Fremdling in Efremovka CAI Ef2. Gray: taenite; 2-10 μm dark inclusions: schreibersite; $\leq 1 \mu\text{m}$ dark inclusions: V-rich magnetite; white inclusions: Mo,W-rich alloy. The outer rim is free of phosphides, magnetite, and Mo,W-rich alloy. The mantle contains magnetite and Mo,W-rich alloy, but no schreibersite. The core contains all phases. Circles show locations of LA-ICP-MS analyses. Scale bar = 100 μm .

Figure 7. X-ray maps of (a) P and (b) V in and near EM2 in Ef2. Ca-phosphate is visible surrounding the Fremdling in the P map. Phosphides are visible in the core; vanadian magnetite is visible in the core, in the mantle, and surrounding the Fremdling; and the rim of the Fremdling is free of P and V. Scale bars = 100 μm .

Figure 8. Siderophile element concentrations in Fremdling EM2 in the Efremovka CAI EF2, measured by LA-ICP-MS. The core (black circles), mantle (open circles), and rim (gray circles) are defined in the captions of Figures 6 and 7.

Figure 9. Siderophile element concentrations in Fremdlings, measured by LA-ICP-MS. (A) Fremdlings in Ef2; (B) Fremdlings in Ef3; (C) Calculated bulk abundances of three large Fremdlings. Data below detection limits are omitted from these figures.

Figure 10. Calculated abundance patterns during condensation from the solar nebula at $P_{\text{H}_2} = 1 \times 10^{-3}$ bar. Legends identify the temperature (K) to which each curve pertains. Elements are listed in order of increasing volatility in the solar nebula. A) 1900-1300 K. B) 1500-1450 K.

Figure 11. Phase diagram for the Fe and Ni endmembers of the schreibersite-whitlockite reaction: $2 (\text{Fe,Ni})_3\text{P} + 3 \text{CaO} + 5/2 \text{O}_2 = 6 (\text{Fe,Ni}) + \text{Ca}_3(\text{PO}_4)_2$. The iron-wüstite buffer (IW) is shown for comparison. Data from Knacke et al. (1991), Barin (1995), and Chase (1998).

Figure 12. a) Re vs. Os for Fremdlinge from Efremovka CAIs. The line shows the chondritic Re/Os ratio. b) Re/Os vs. Os for Efremovka CAIs. Line: the chondritic Re/Os ratio (Anders and Grevesse, 1989); dashed line: 2x CI value. EM18 (Ef2), which was altered by phosphidation (see text), and EM15 (Ef3), which has a large error for Re, are not depicted.

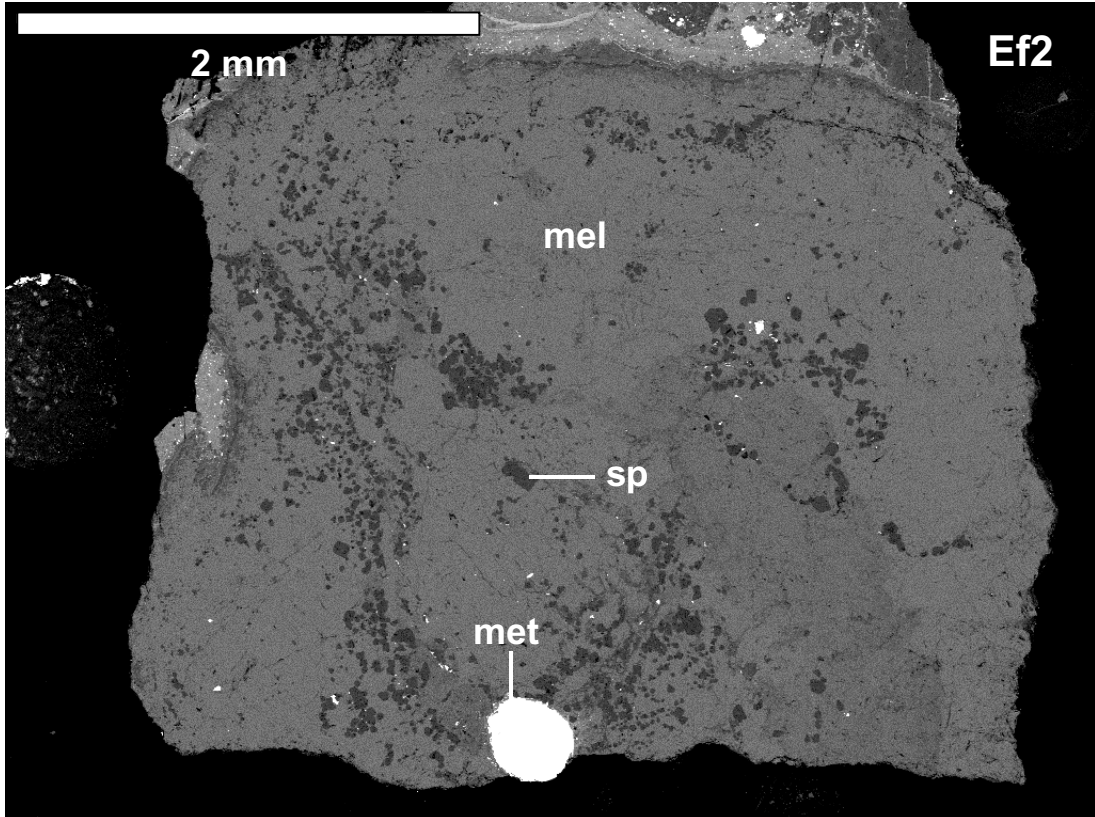


Figure 1

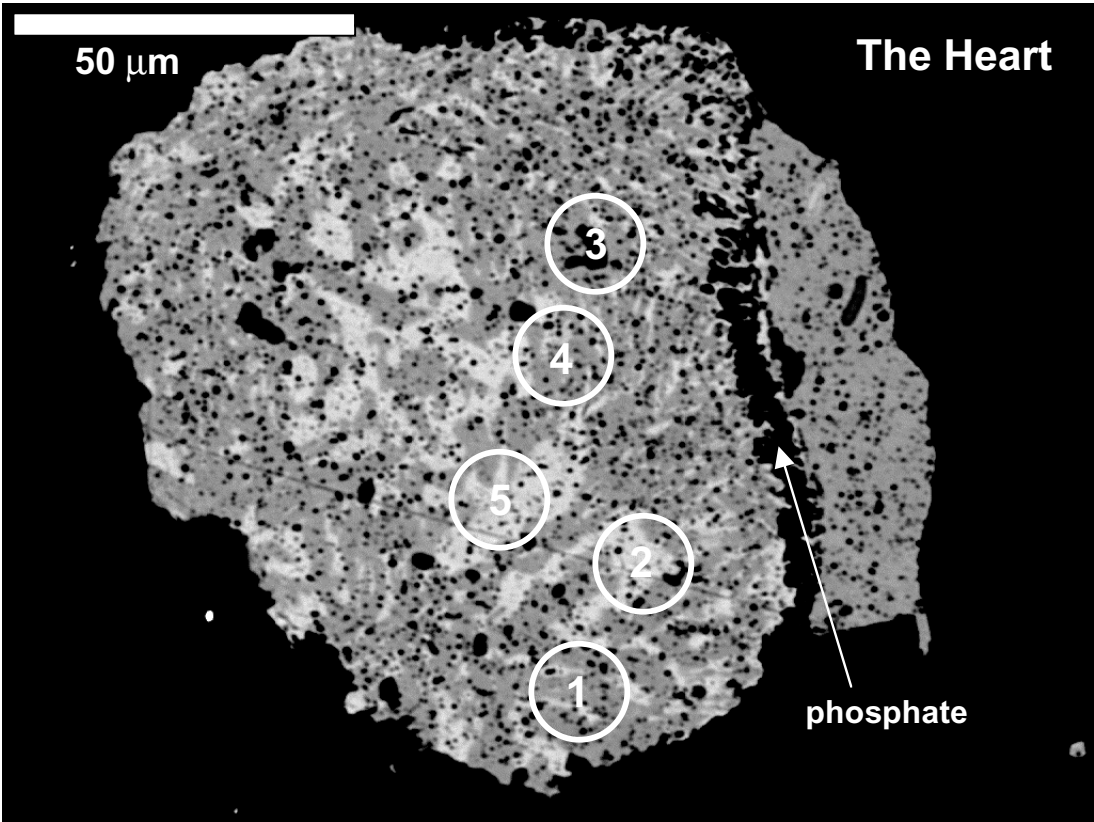


Figure 2

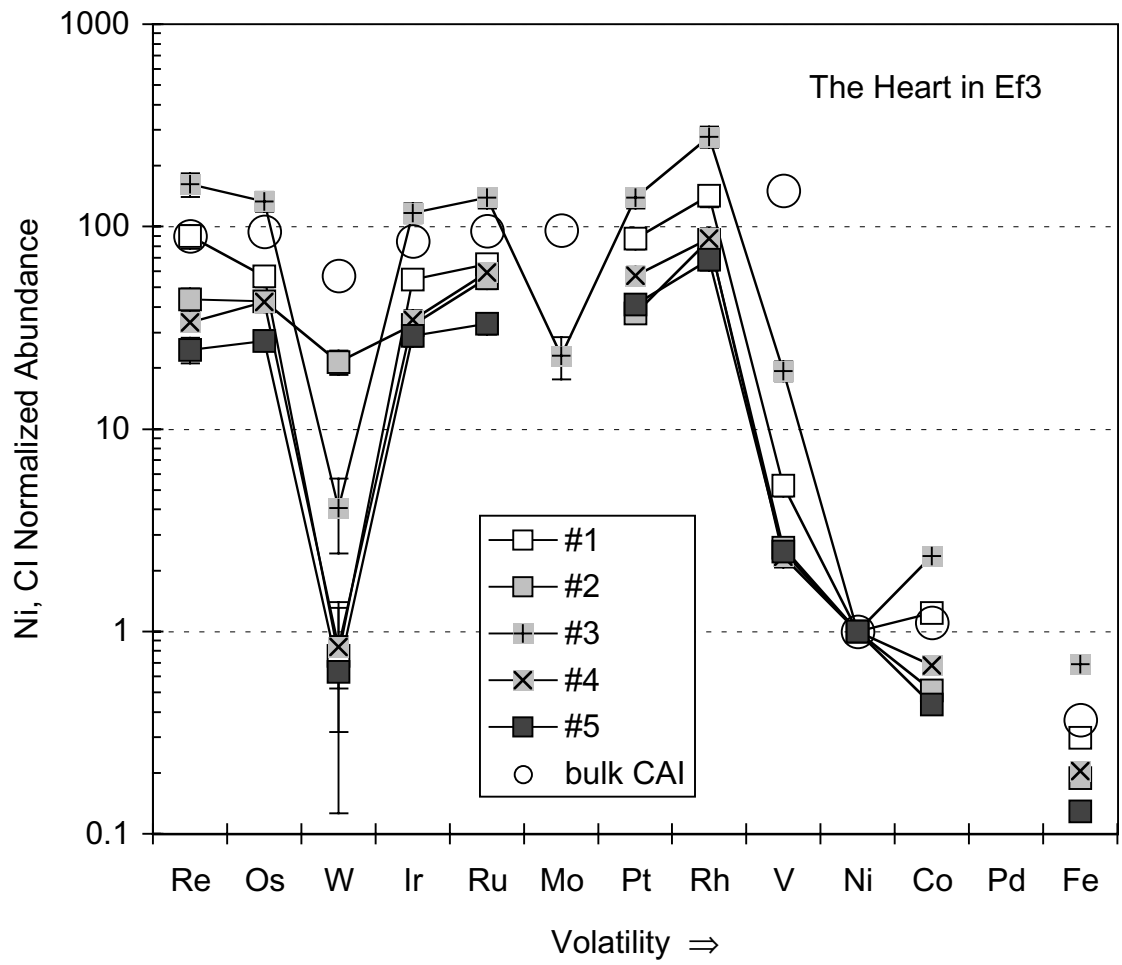


Figure 3

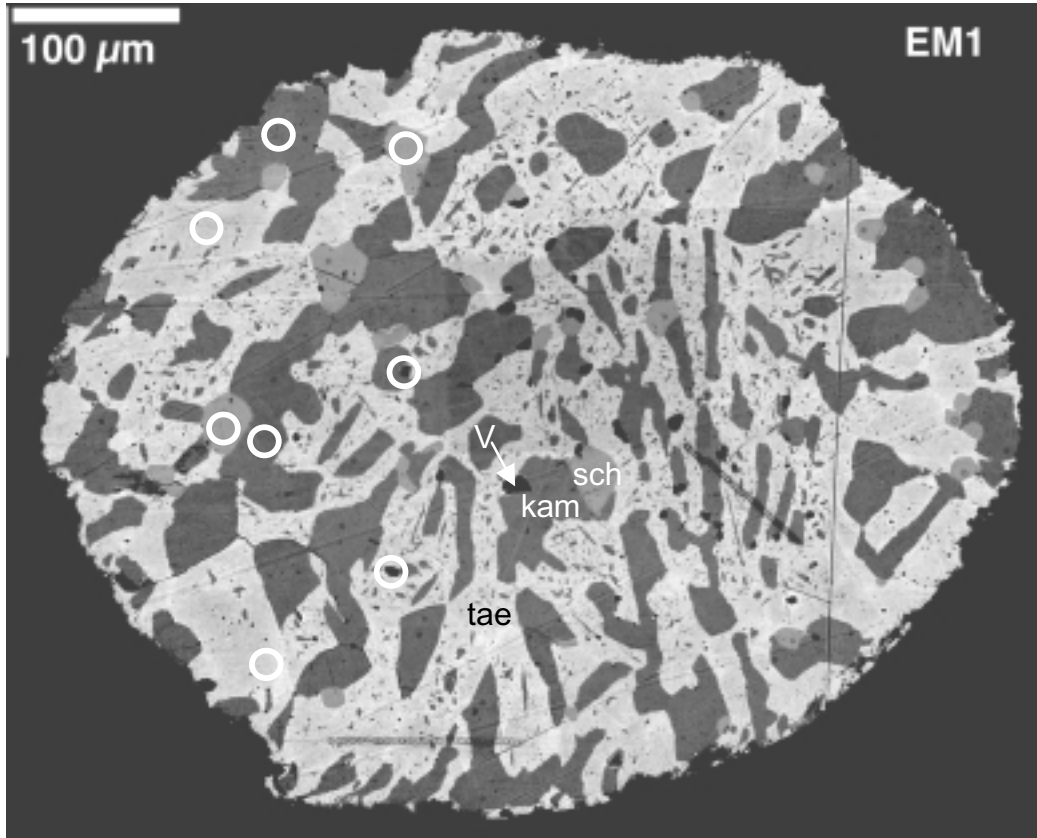


Figure 4

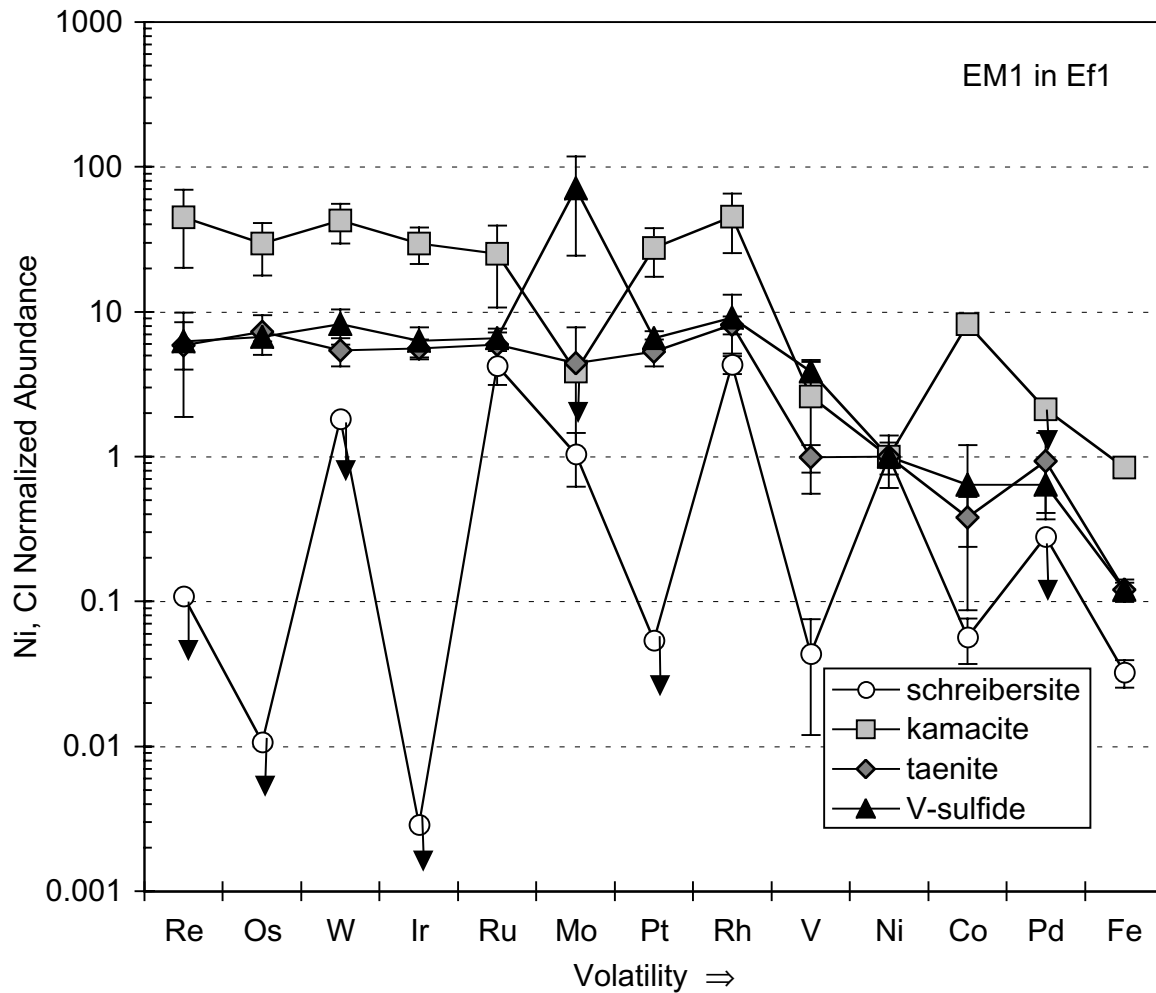


Figure 5

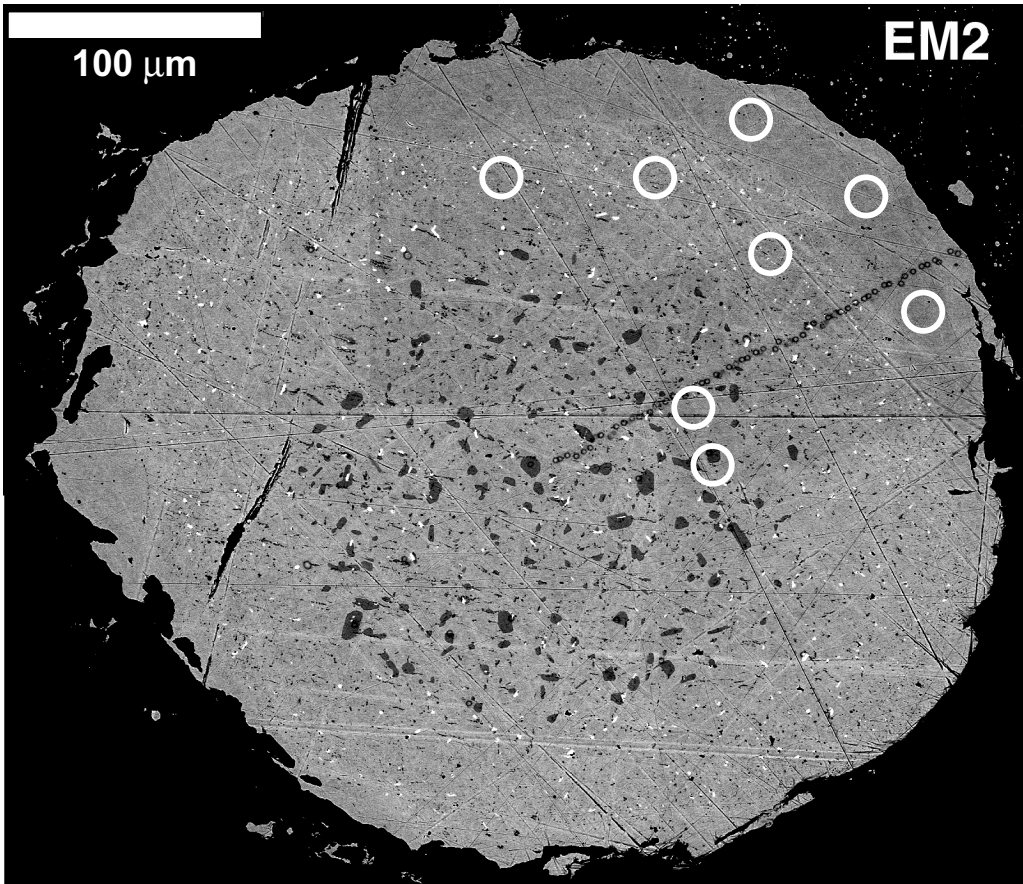


Figure 6

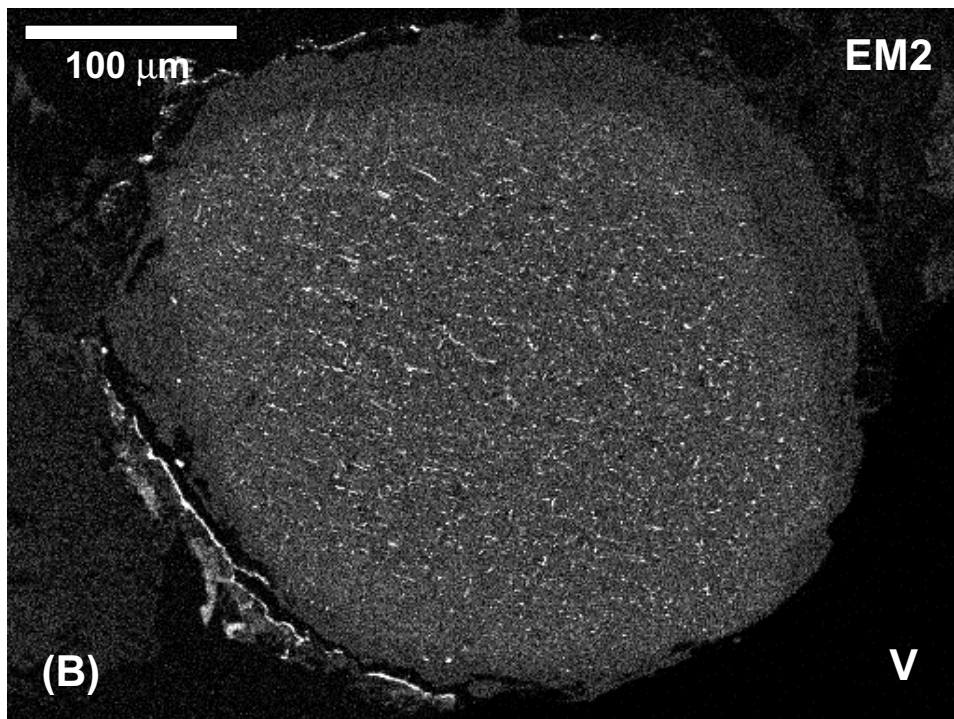
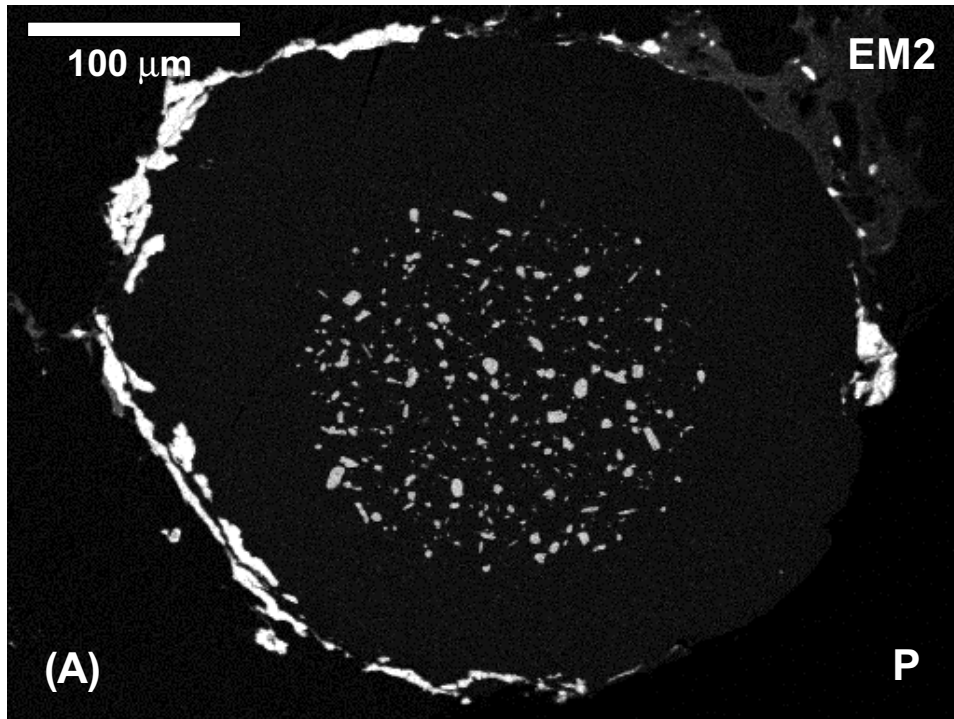


Figure 7

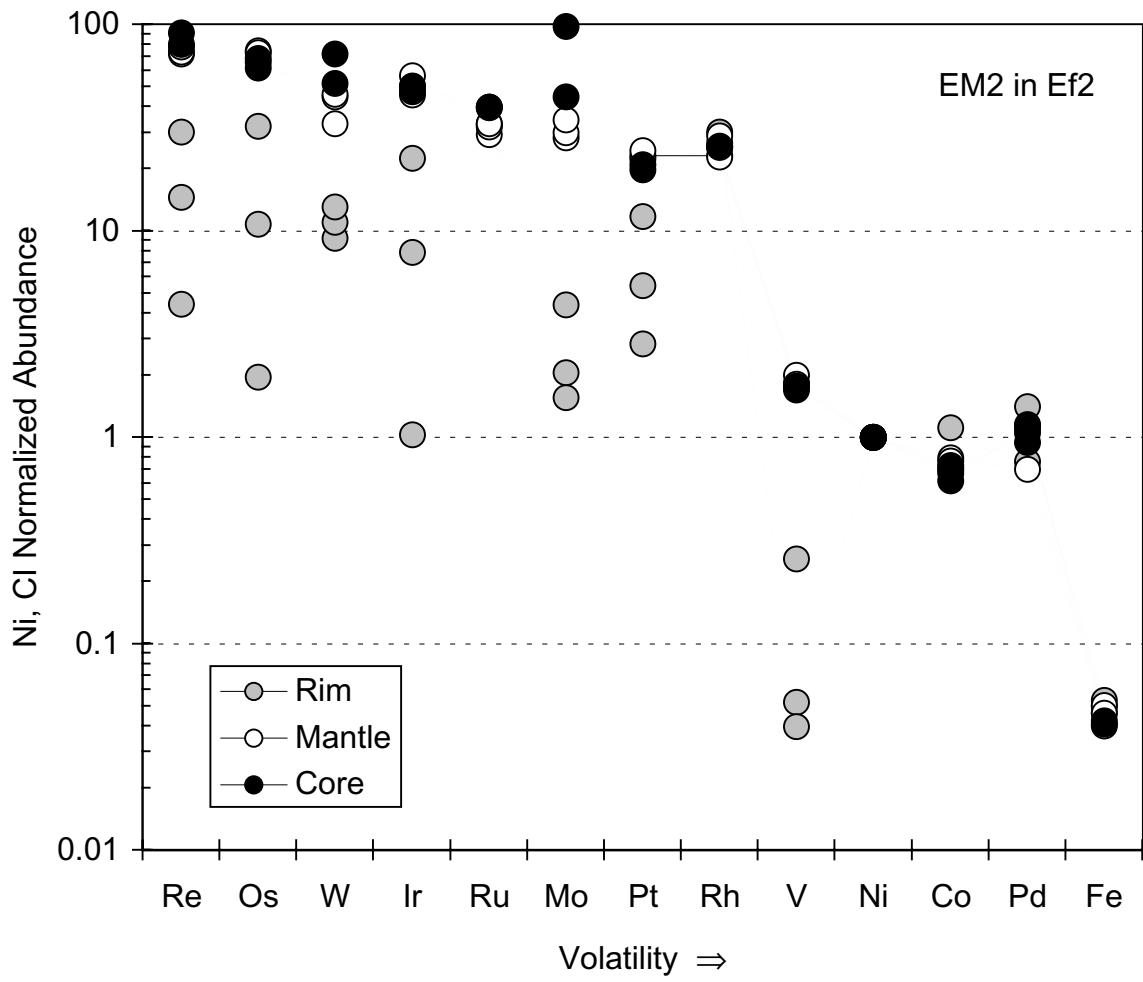


Figure 8

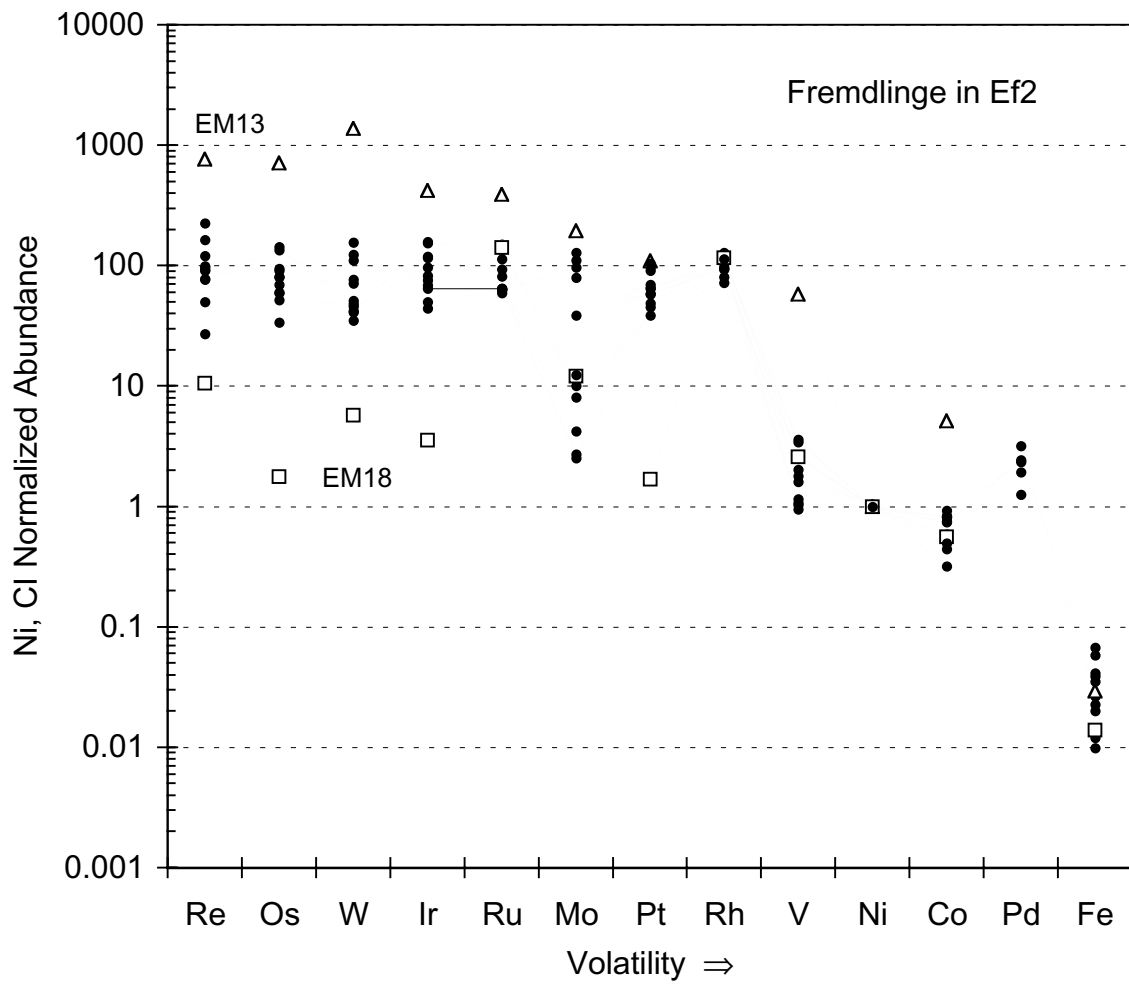


Figure 9 A

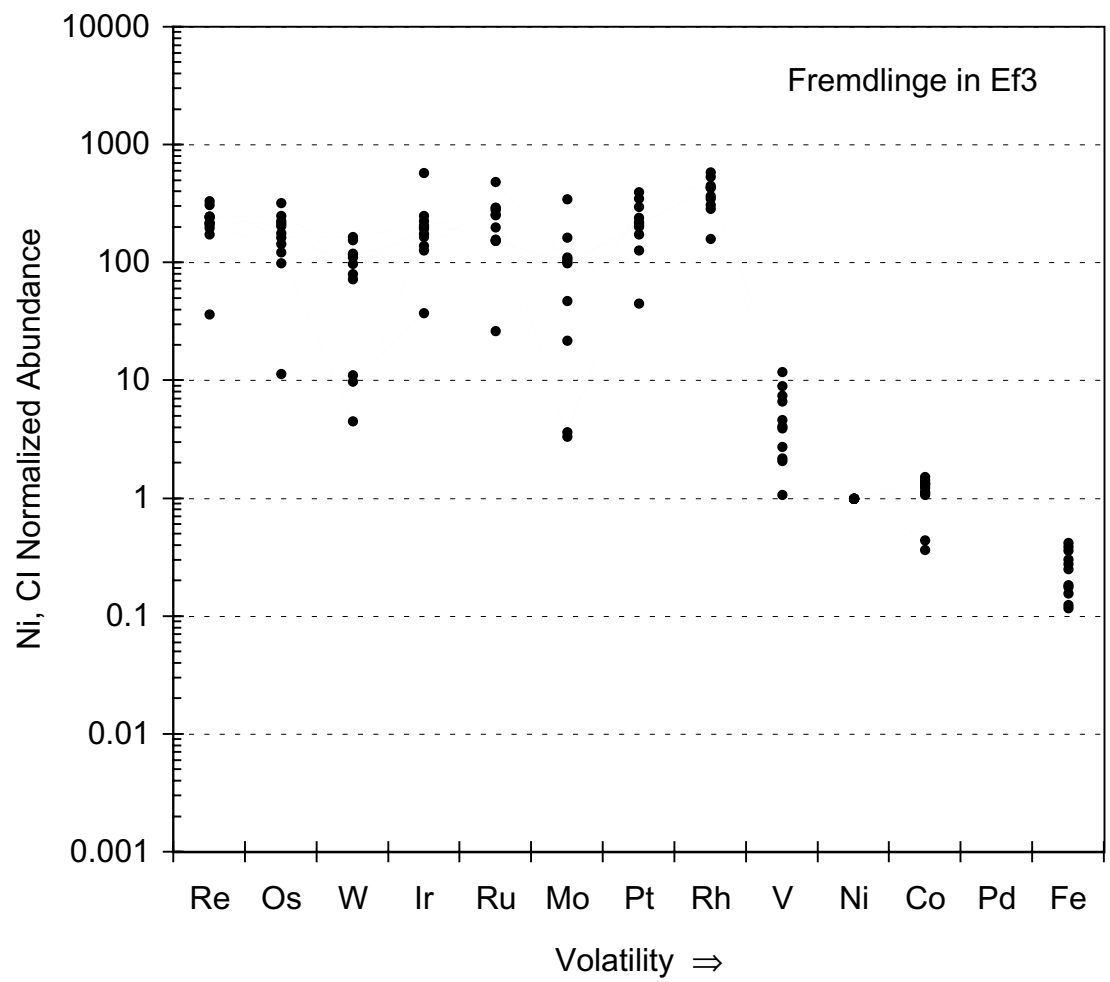


Figure 9 B

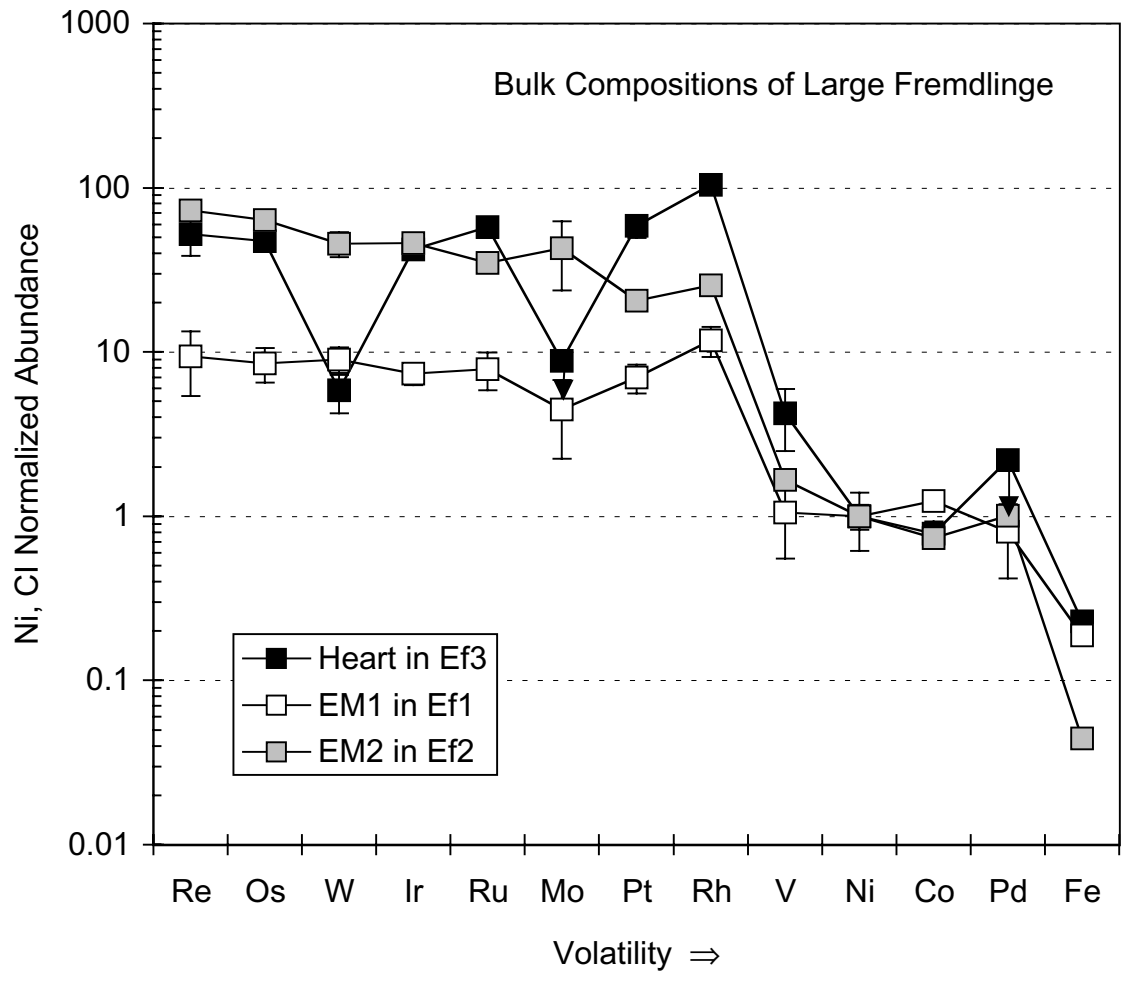


Figure 9 C

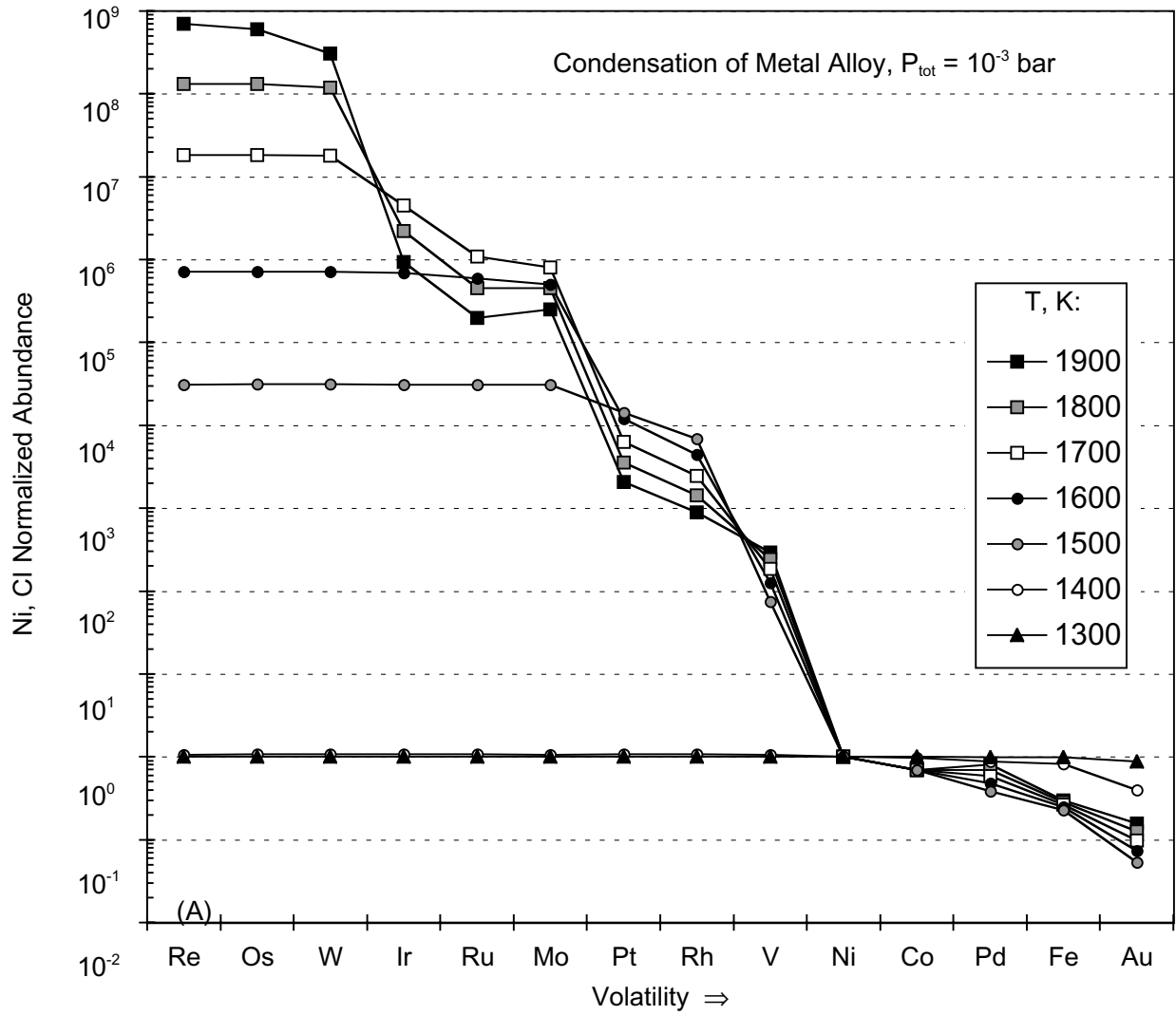


Figure 10 A

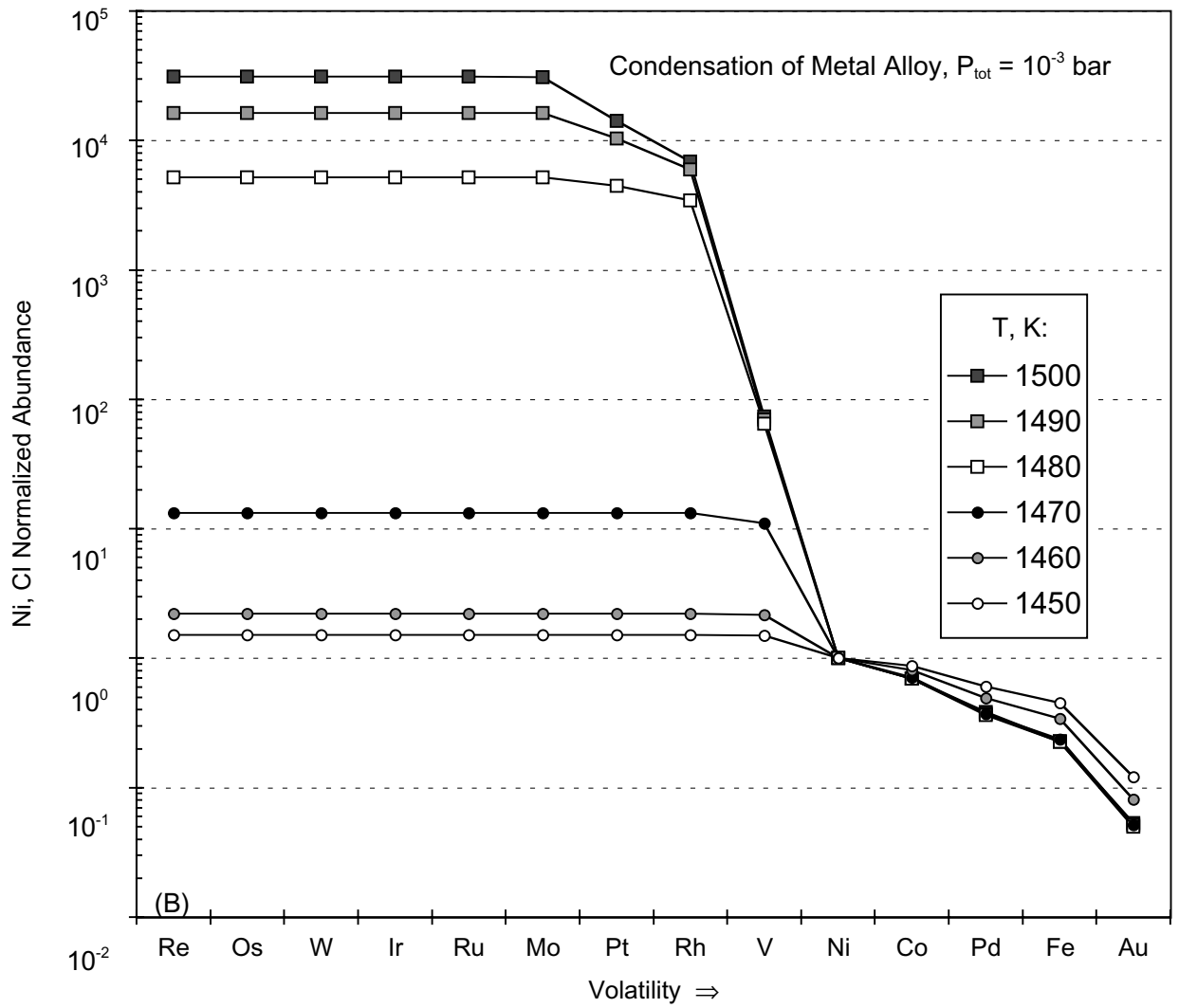


Figure 10 B

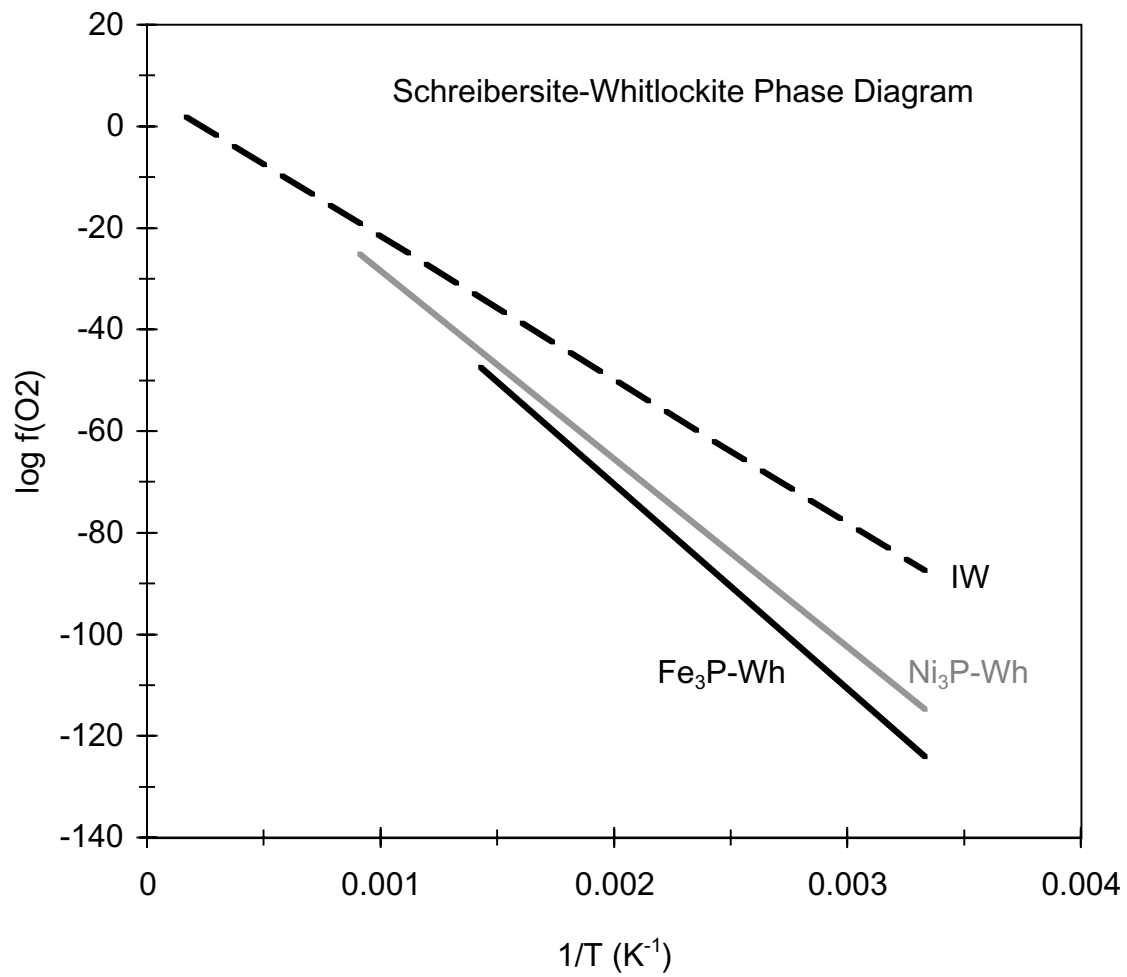


Figure 11

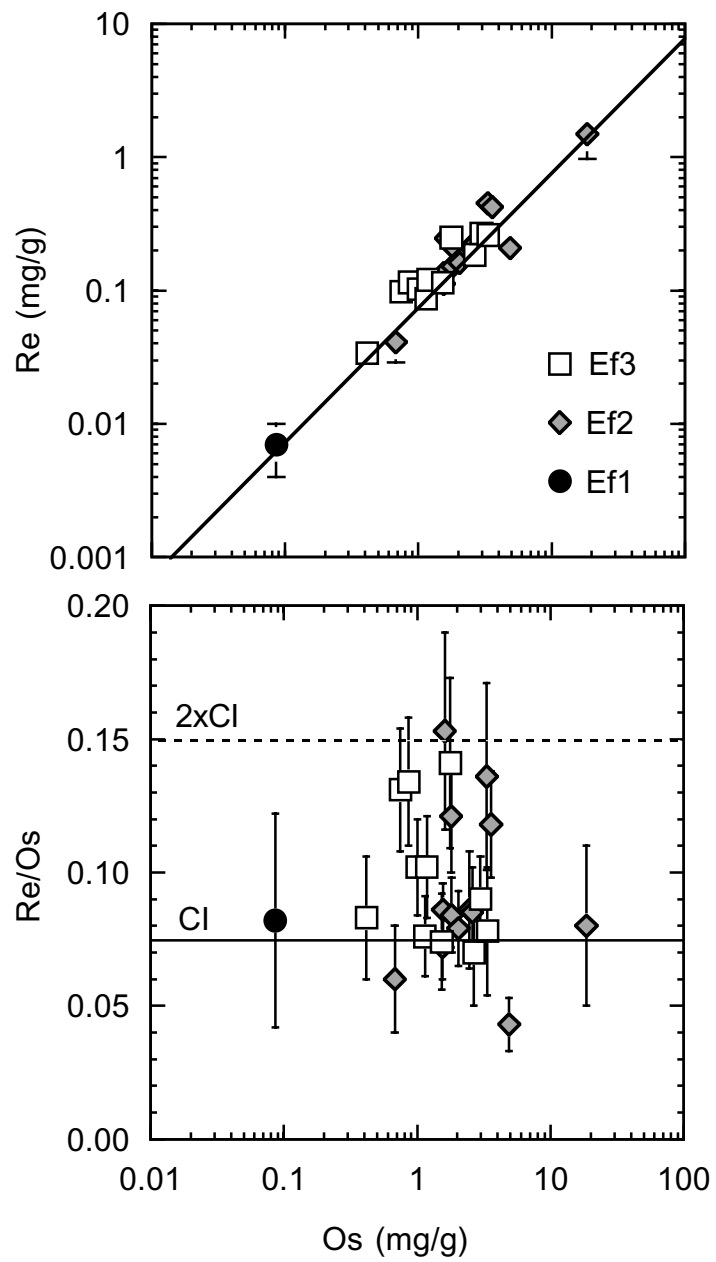


Figure 12